A KINETIC MODEL FOR THE SEDIMENTATION OF ROD–LIKE PARTICLES

CHRISTIANE HELZEL* AND ATHANASIOS E. TZAVARAS†‡

Abstract. We consider a coupled system consisting of a kinetic equation coupled to a macroscopic Stokes (or Navier-Stokes) equation and describing the motion of a suspension of rigid rods in gravity. A reciprocal coupling leads to the formation of clusters: The buoyancy force creates a macroscopic velocity gradient that causes the microscopic particles to align so that their sedimentation reinforces the formation of clusters of higher particle density. We provide a quantitative analysis of cluster formation. We derive a nonlinear moment closure model, which consists of evolution equations for the density and second order moments and that uses the structure of spherical harmonics to suggest a closure strategy. For a rectilinear flow we employ the moment closure together with a quasi-dynamic approximation to derive an effective equation. The effective equation is an advection-diffusion equation with nonisotropic diffusion coupled to a Poisson equation, and belongs to the class of the so-called flux-limited Keller-Segel models. For shear flows, we provide an argument for the validity of the effective equation and perform numerical comparisons that indicate good agreement between the original system and the effective theory. For rectilinear flow we show numerical results which indicate that the quasi-dynamic provides accurate approximations. Finally, a linear stability analysis on the moment system shows that linear theory predicts a wavelength selection mechanism for the cluster width, provided that the Reynolds number is larger than zero.

Key words. sedimentation, rod-like particles, moment closure, quasi-dynamic approximation, linear stability

AMS subject classifications. 76T20, 74A25, 35B40, 35B35, 35B36

1. Introduction. Complex fluids with suspended microstructure might include diverse materials such as polymeric solutions with a long chain structure, or suspensions of non-deformable particles with an orientation (for example rod-like particles). Such systems might be modeled via continuum modeling of viscoelastic fluids, or via mesoscopic models within the realm of kinetic theory, or even as particles in a fluid. Multi-scale interactions cause interesting phenomena in the dynamics of complex flows, and the area forms an interesting testing ground for examining the effect of change of scale and the passage from microscopic to mesoscopic to macroscopic theories.

An interesting system is offered by a suspension of rod-like particles in a dilute solution under the influence of gravity. For such a system, the macroscopic flow can cause a change of orientation for the suspended microstructure, which in turn, produces an elastic stress that interacts with and modifies the macroscopic flow. The sedimentation of dilute suspensions of rod-like particles can lead to cluster formations and has been studied by several authors in theoretical, numerical and experimental work, see the recent review paper by Guazzelli and Hinch [8] and references therein.

Experimental works by Guazzelli and coworkers [13, 14, 21] reveal the following scenarios: Starting from a well-stirred suspension packets of particles form after some time. These packets seem to have a mesoscopic equilibrium width, suggesting that the density of particles acquires variations of a characteristic length scale. Within a cluster, individual particles are aligned with the direction of gravity during most of the time; occasionally they flip. The average settling speed in a suspension is larger than the sedimentation speed of a single particle oriented in the direction of gravity. The mechanism of cluster formation was described in a fundamental paper of Koch and Shaqfeh [19]. In recent years the sedimentation of rod-like (and other orientable) particles has also been studied via numerical simulations of multi-scale models. Gustavsson and Tornberg [29, 9] used a very detailed description of rod-like particles in a dilute suspension based on a slender body approximation. They were able to simulate suspensions with up to a few hundred particles and a domain size of the order of a few particle length. Butler and Shaqfeh [2] used a lower order slender body description. Saintillan et al. [25] accelerated this algorithm using fast summation techniques. This allowed them to simulate several thousand particles. Wang and Layton [31] used the immersed boundary method for their two-dimensional numerical studies. All numerical studies confirm the basic experimental findings: Packet formation and alignment in gravity direction. Note that the models used in those simulations are of more microscopic nature than the model considered here. Instead of a number density function for the rod orientation in every point

*Institute of Mathematics, Heinrich-Heine-University Düsseldorf, Düsseldorf, Germany, christiane.helzel@hhu.de

†Computer, Electrical, Mathematical Sciences & Engineering Division, King Abdullah University of Science and Technology (KAUST), Thuwal, Saudi Arabia, athanasios.tzavaras@kaust.edu.sa

‡Institute of Applied and Computational Mathematics, FORTH, Heraklion, Greece.

of the domain, those authors model a large number of individual particles. Moreover, Brownian effects are not considered in those models.

Our objective here is to provide a quantitative description of cluster formation by deriving an effective theory via asymptotic methods. We focus on a multi-scale model that in non-dimensional form reads

$$\begin{aligned} \partial_t f + \nabla_{\boldsymbol{x}} \cdot (\boldsymbol{u} f) + \nabla_{\boldsymbol{n}} \cdot (P_{\boldsymbol{n}^\perp} \nabla_{\boldsymbol{x}} \boldsymbol{u} \boldsymbol{n} f) - \nabla_{\boldsymbol{x}} \cdot ((I + \boldsymbol{n} \otimes \boldsymbol{n}) \boldsymbol{e}_3 f) \\ = D_r \Delta_{\boldsymbol{n}} f + \gamma \nabla_{\boldsymbol{x}} \cdot (I + \boldsymbol{n} \otimes \boldsymbol{n}) \nabla_{\boldsymbol{x}} f \\ \sigma = \int_{S^{d-1}} (d\boldsymbol{n} \otimes \boldsymbol{n} - I) f \, d\boldsymbol{n} \\ Re \, (\partial_t \boldsymbol{u} + (\boldsymbol{u} \cdot \nabla_{\boldsymbol{x}}) \boldsymbol{u}) = \Delta_{\boldsymbol{x}} \boldsymbol{u} - \nabla_{\boldsymbol{x}} p + \delta \gamma \nabla_{\boldsymbol{x}} \cdot \sigma - \delta \int_{S^{d-1}} f \, d\boldsymbol{n} \boldsymbol{e}_3 \\ \nabla_{\boldsymbol{x}} \cdot \boldsymbol{u} = 0 \, . \end{aligned} \tag{1.1}$$

Here, $f(t, \boldsymbol{x}, \boldsymbol{n})$ describes the distribution function of particles as a function of time t, space $\boldsymbol{x} \in \mathbb{R}^d$ and the orientation of the rod-like particles $\boldsymbol{n} \in S^{d-1}$, $\boldsymbol{u}(t, \boldsymbol{x})$ stands for the velocity of the solvent, $p(t, \boldsymbol{x})$ is the pressure, while D_r, γ, δ and Re stand for non-dimensional numbers (see Section 2.2). The model, described in detail in Section 2, puts together in a context of dilute suspensions of rod-like particles various elements described in the book of Doi and Edwards [5]. Such kinetic models for complex fluids hinge on hydrodynamical models for suspensions modeled by Fokker-Planck equations [15, 16] and have a remarkable thermodynamical structure [5, Sec 8.6]. Similar models are studied in [23, 11] in connection to shear band formation in polymeric flows. We note that the factors that lead, according to Koch and Shaqfeh [19], to the instability of the sedimentation process are included in this model, and the cluster formation mechanism is described in section 2.3.

Due to the high-dimensionality of the problem, numerical computations of the full five dimensional problem (for $d = 3$) are cumbersome. We are therefore interested in the derivation of partial differential equations (pdes), which describe the macroscopic flow without resolving the microscopic structure. Such nonlinear models should also provide further insight into the basic nonlinear mechanism which leads to cluster formation. Sections 3 and 4 are devoted to the derivation of such simpler pde models. In Section 3, we perform a moment closure from the full multi-scale model, based on deriving equations for the moments, and using the structure of spherical harmonics to suggest a closure strategy. We adapt the results to various special flows of interest, including rectilinear flows and shear flows. The obtained models (3.9) and (3.6) have some analogies to the familiar Oldroyd-B models in continuum viscoelasticity (see Renardy [22] for a description and further references).

The moment closure leads to a d-dimensional system of pdes (1-dimensional for shear flow, 2-dimensional for rectilinear flow) and thus reduces the dimension of the problem. A second approximation, explained in Section 4, leads to a scalar evolution equation for the particle density coupled to the equation of the flow and provides an even simpler description of the process of cluster formation. We call this quasi-dynamic approximation and it consists of setting the higher order moments to their local equilibrium and evaluating them in terms of the zero-th moment and its spatial derivatives. It leads to an emerging effective equation for the particle density. For the case of rectilinear flow along the z-direction of the three-dimensional space $\boldsymbol{x} = (x, y, z)$, with ansatz

$$f = f(t, x, y, \boldsymbol{n}) \, , \quad \boldsymbol{u} = \big(0, 0, w(t, x, y)\big)^T \, ,$$

the resulting effective system reads

$$\begin{aligned} \partial_t \rho = \nabla \cdot \left(\frac{1}{\kappa + 10 |\nabla w|^2} \left[I - \frac{36 |\nabla w|^2}{\kappa + 46 |\nabla w|^2} \, \frac{\nabla w}{|\nabla w|} \otimes \frac{\nabla w}{|\nabla w|} \right] \tfrac{\kappa}{30} \rho \nabla \big(w + \tfrac{1}{3} \ln \rho \big) \right) \\ Re \, \partial_t w = \triangle_{(x,y)} w + \delta \, (\bar{\rho} - \rho) \end{aligned} \tag{1.2}$$

where $\rho = \int f d\boldsymbol{n}$ and $\kappa = 42^2$.

The system (1.2) should be compared to the Keller-Segel model (*e.g.* [18, 12, 1]) used as a model for chemotaxis. There are two differences: (a) that the diffusion in $(1.2)_1$ is anisotropic; more important

(b) that both convection and diffusion are flux-limited, thus making the system belong to the general type of flux-limited chemotaxis systems (*e.g* [6, 30, 24]).

We discuss in Sections 4.4 and 4.5 the nature of the quasi-dynamic approximation and provide some justifying arguments. For the case of shear flows, an eigenvalues analysis of a linearized system suggests that the approximation should be valid for moderate strain rates. Moreover, numerical simulations for shear flows confirm that the solution structure obtained from the scalar evolution equation agrees very well with the solution structure of the full model. Numerical results for rectilinear flow show a good agreement between the nonlinear moment closure model and the quasi-dynamic approximation.

In appendix A, we summarise properties of the spherical harmonics, that are extensively used throughout this work. In appendix B, we present results of a linear stability analysis for shear flows. In particular, we show that linear stability theory predicts a wavelength selection only if the Reynolds number of the macroscopic flow is larger than zero.

2. The mathematical model. We describe a kinetic model for sedimentation in dilute suspensions of rod-like Brownian particles. Models of this type were introduced by Doi and Edwards, see [5, Ch. 8]. In [23] and [11] a related model for suspensions of rod-like particles was considered. This model is extended here to account for the effects of gravity in an effort to describe sedimentation of rod-like particles in a solvent.

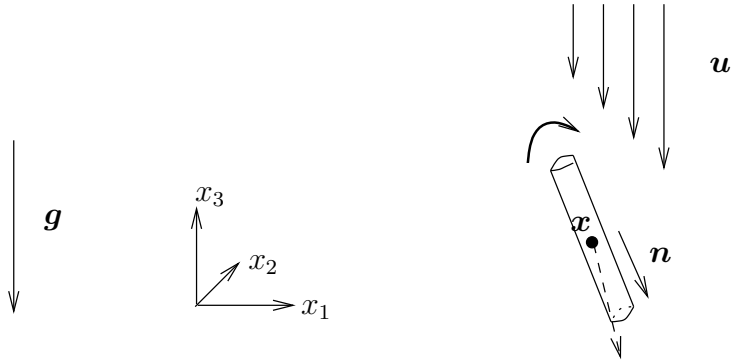

FIG. 2.1. *Basic notation for rod-like molecule which is falling sidewards.*

We consider inflexible rod-like particles of thickness b which is much smaller than the particles length l. Our considerations are restricted to the dilute regime which is characterised by the relation $\nu \ll l^{-3}$ where ν is the number density. Note that in contrast to the model considered in [23], the number density is not constant here. The orientation of a rod-like particle is characterised by $\boldsymbol{n} \in S^{d-1}$ where d is the dimension of the macroscopic physical space $\Omega \subset \mathbb{R}^d$. While the assumptions for the dilute regime are satisfied for the well stirred dilute suspension of rod-like particles, at a later time the assumption might be violated inside a cluster after particles have concentrated there. It would be interesting to switch to a semi-dilute or concentrated model inside a cluster. We hope to consider such extensions of the model in forthcoming work. However, we believe that the dilute model is appropriate to study the initial stages of cluster formation.

We denote by $\boldsymbol{e}_3$ the unit vector in the upward direction and by $\boldsymbol{g} = -g\boldsymbol{e}_3$ the acceleration of gravity with gravitational constant g. Furthermore, let m_0 denote the mass of an individual rod-like particle and $\boldsymbol{G} = -m_0 g \boldsymbol{e}_3$ be the force of gravity on a single particle. Some of our basic notation is depicted in Figure 2.1.

In a quiescent suspension (i.e. macroscopic velocity $\boldsymbol{u} = 0$) each particle sediments at a speed

depending on its orientation $\boldsymbol{n}$ according to

$$\begin{aligned}\frac{d\boldsymbol{x}}{dt} &= \frac{1}{\zeta_{||}}\left(\boldsymbol{G}\cdot\boldsymbol{n}\right)\boldsymbol{n} + \frac{1}{\zeta_{\perp}}\left(\boldsymbol{G} - \left(\boldsymbol{G}\cdot\boldsymbol{n}\right)\boldsymbol{n}\right)\\ &= \left(\frac{1}{\zeta_{||}}\boldsymbol{n}\otimes\boldsymbol{n} + \frac{1}{\zeta_{\perp}}\left(I - \boldsymbol{n}\otimes\boldsymbol{n}\right)\right)\boldsymbol{G}\\ &= \frac{1}{\zeta_{\perp}}\left(\boldsymbol{n}\otimes\boldsymbol{n} + I\right)\boldsymbol{G}\end{aligned}$$

where $\zeta_{||}$ and $\zeta_{\perp}$ are the frictional coefficients in the tangential and the normal direction. On the basis of the Kirkwood theory $\zeta_{||}$, $\zeta_{\perp}$ satisfy $\zeta_{\perp} = 2\zeta_{||}$, see [5, App 8.I]. In particular, a particle with a horizontal orientation sediments slower than a particle with a vertical orientation and a particle of oblique orientation moves also sideways.

In addition a macroscopic velocity gradient causes a rotation according to the equation

$$\frac{d\boldsymbol{n}}{dt} = P_{\boldsymbol{n}^{\perp}}\nabla_{\boldsymbol{x}}\boldsymbol{u}\boldsymbol{n}$$

where $P_{\boldsymbol{n}^{\perp}}\nabla_{\boldsymbol{x}}\boldsymbol{u}\boldsymbol{n} := \nabla_{\boldsymbol{x}}\boldsymbol{u}\boldsymbol{n} - \left(\nabla_{\boldsymbol{x}}\boldsymbol{u}\boldsymbol{n}\cdot\boldsymbol{n}\right)\boldsymbol{n}$ is the projection of the vector $\nabla_{\boldsymbol{x}}\boldsymbol{u}\boldsymbol{n}$ on the tangent space at $\boldsymbol{n}$.

We next include the effects of rotational and translational Brownian motion and account for the macroscopic mean flow $\boldsymbol{u}(\boldsymbol{x},t)$. The model then becomes the system of stochastic differential equations

$$\begin{aligned}d\boldsymbol{x} &= \boldsymbol{u}dt + \left(\frac{1}{\zeta_{||}}\boldsymbol{n}\otimes\boldsymbol{n} + \frac{1}{\zeta_{\perp}}\left(I - \boldsymbol{n}\otimes\boldsymbol{n}\right)\right)\boldsymbol{G}\,dt\\ &\quad + \sqrt{\frac{2k_B\theta}{\zeta_{||}}\boldsymbol{n}\otimes\boldsymbol{n} + \frac{2k_B\theta}{\zeta_{\perp}}\left(I - \boldsymbol{n}\otimes\boldsymbol{n}\right)}\,dW\\ d\boldsymbol{n} &= P_{\boldsymbol{n}^{\perp}}\nabla_{\boldsymbol{x}}\boldsymbol{u}\boldsymbol{n}\,dt + \sqrt{\frac{2k_B\theta}{\zeta_r}}\,dB\end{aligned} \tag{2.1}$$

where W is the translational Brownian motion and B is the rotational Brownian motion, ζ_r is the rotational friction coefficient, k_B is the Boltzmann constant and θ the absolute temperature. The definition of the translational Brownian motion dW is classical, while the definition of the rotational Brownian motion dB requires analysis of geometric flavor, see [7, 17].

The above stochastic equations may be equivalently expressed via the Smoluchowski equation for the evolution of the *local orientational distribution function*:

$$\begin{aligned}&\partial_t f + \nabla_{\boldsymbol{x}}\cdot\left[\left(\boldsymbol{u} + \frac{1}{\zeta_{\perp}}\left(\boldsymbol{n}\otimes\boldsymbol{n} + I\right)\left(-m_0 g\boldsymbol{e}_3\right)\right)f\right] + \nabla_{\boldsymbol{n}}\cdot\left(P_{\boldsymbol{n}^{\perp}}\nabla_{\boldsymbol{x}}\boldsymbol{u}\boldsymbol{n}f\right)\\ &\quad = \frac{k_B\theta}{\zeta_r}\Delta_{\boldsymbol{n}}f + \frac{k_B\theta}{\zeta_{\perp}}\nabla_{\boldsymbol{x}}\cdot\left(\boldsymbol{n}\otimes\boldsymbol{n} + I\right)\nabla_{\boldsymbol{x}}f.\end{aligned} \tag{2.2}$$

Here $f(\boldsymbol{x},t,\boldsymbol{n})\,d\boldsymbol{n}$ describes the number of particles per unit volume at macroscopic position $\boldsymbol{x}$ and time t with orientations in the element centered at $\boldsymbol{n}$ and of volume $d\boldsymbol{n}$. The second term on the left hand side of (2.2) models transport of the center of mass of the particles due to the macroscopic flow velocity and due to gravity. The last term on the left hand side models the rotation of the axis due to a macroscopic velocity gradient $\nabla_{\boldsymbol{x}}\boldsymbol{u}$. The terms on the right hand side describe rotational as well as translational diffusion. They together amount to non-isotropic spatial diffusion, which is one of the main features of the model at hand. The gradient, divergence and Laplacian on the sphere are denoted by $\nabla_{\boldsymbol{n}}$, $\nabla_{\boldsymbol{n}}\cdot$ and $\Delta_{\boldsymbol{n}}$, while the gradient and divergence in the macroscopic flow domain are denoted by $\nabla_{\boldsymbol{x}}$ and $\nabla_{\boldsymbol{x}}\cdot$. The total number of rod-like particles is

$$\int_{\Omega}\int_{S^{d-1}} f(\boldsymbol{x},t,\boldsymbol{n})\,d\boldsymbol{n}\,d\boldsymbol{x} = \int_{\Omega}\int_{S^{d-1}} f(\boldsymbol{x},0,\boldsymbol{n})\,d\boldsymbol{n}\,d\boldsymbol{x} = N,$$

i.e. f has dimensions of number density. It is convenient to rewrite the Smoluchowski equation in the form

$$\begin{aligned}\partial_t f + \nabla_{\boldsymbol{x}} \cdot (\boldsymbol{u} f) + \nabla_{\boldsymbol{n}} \cdot (P_{\boldsymbol{n}^\perp} \nabla_{\boldsymbol{x}} \boldsymbol{u} \boldsymbol{n} f) \\ = D_r \Delta_{\boldsymbol{n}} f + D_\perp \nabla_{\boldsymbol{x}} \cdot (I + \boldsymbol{n} \otimes \boldsymbol{n}) \Big(\nabla_{\boldsymbol{x}} f + \frac{1}{k_B \theta} f \, \nabla_{\boldsymbol{x}} U \Big),\end{aligned} \tag{2.3}$$

where $D_r := \frac{k_B \theta}{\zeta_r}$ and $D_\perp := \frac{k_B \theta}{\zeta_\perp}$ stand for the rotational and translational diffusion coefficients and $U(x) = m_0 g(\boldsymbol{x} \cdot \boldsymbol{e}_3)$ is the potential of the gravity force $\boldsymbol{G} = -\nabla U = -m_0 g \boldsymbol{e}_3$. The reader is referred to [17, Ch 1 & Ch 3] for the Ito calculus required to establish the relation between the stochastic differential equation (2.1) and the kinetic equation (2.3). In the sequel, we work with equation (2.3).

As can be seen from (2.3), a velocity gradient $\nabla_{\boldsymbol{x}} \boldsymbol{u}$ distorts an isotropic distribution f which leads to an increase in entropy. Thermodynamic consistency requires that this is balanced by a stress tensor $\sigma(\boldsymbol{x}, t)$ given by

$$\sigma(\boldsymbol{x}, t) := k_B \theta \int_{S^{d-1}} (d\boldsymbol{n} \otimes \boldsymbol{n} - I) \, f(\boldsymbol{x}, t, \boldsymbol{n}) d\boldsymbol{n}. \tag{2.4}$$

(see [5, Sec 8.6] and compare with Section 2.1).

Local variations in the density $m_0 \int_{S^{d-1}} f d\boldsymbol{n}$ lead to spatial variations of the specific weight of the suspension that generally can not be compensated by a hydrostatic pressure and thus trigger a fluid motion (buoyancy). The macroscopic flow is described by the Navier-Stokes equation. Let ρ_f be the density of the fluid which is assumed to be constant. The balance laws of mass and momentum have the form

$$\begin{aligned}\rho_f \Big[\partial_t \boldsymbol{u} + (\boldsymbol{u} \cdot \nabla_{\boldsymbol{x}}) \, \boldsymbol{u} \Big] = \mu \triangle_{\boldsymbol{x}} \boldsymbol{u} - \nabla_{\boldsymbol{x}} p + \nabla_{\boldsymbol{x}} \cdot \sigma \\ - \rho_f g \boldsymbol{e}_3 - \Big(\int_{S^{d-1}} f d\boldsymbol{n} \Big) m_0 g \boldsymbol{e}_3 \\ \nabla_{\boldsymbol{x}} \cdot \boldsymbol{u} = 0\end{aligned} \tag{2.5}$$

The coupling between the kinetic equation and the macroscopic flow is effected through the viscoelastic stress σ in (2.4) and the buoyancy of the rods (the last term in (2.5). One might also include an effect of viscous forces induced by the rods, see [15] and [5, Sec 8.6.1]; such an effect is neglected here.

The term $\rho_f g \boldsymbol{e}_3$ can be incorporated to the pressure. For the linear stability analysis it will be convenient to express the momentum equation in the equivalent form

$$\begin{aligned}\rho_f \left(\partial_t \boldsymbol{u} + (\boldsymbol{u} \cdot \nabla_{\boldsymbol{x}}) \, \boldsymbol{u} \right) = \mu \Delta_{\boldsymbol{x}} \boldsymbol{u} - \nabla_{\boldsymbol{x}} p' + \nabla_{\boldsymbol{x}} \cdot \sigma + \left(\frac{N}{V} - \int_{S^{d-1}} f \, d\boldsymbol{n} \right) m_0 g \boldsymbol{e}_3 \\ \nabla_{\boldsymbol{x}} \cdot \boldsymbol{u} = 0\end{aligned} \tag{2.6}$$

by redefining the pressure,

$$p' = p + \rho_f g \boldsymbol{e}_3 \cdot \boldsymbol{x} + \frac{m_0 N g}{V} \boldsymbol{e}_3 \cdot \boldsymbol{x} \, ,$$

to account for the hydrostatic pressures, where V is the volume occupied by the suspension and N the total number of rod-like particles.

We summarise the final model :

$$\begin{aligned}\partial_t f = -\nabla_{\boldsymbol{x}} \cdot (\boldsymbol{u} f) - \nabla_{\boldsymbol{n}} \cdot (P_{\boldsymbol{n}^\perp} \nabla_{\boldsymbol{x}} \boldsymbol{u} \boldsymbol{n} f) + D_r \Delta_{\boldsymbol{n}} f \\ + D_\perp \nabla_{\boldsymbol{x}} \cdot (I + \boldsymbol{n} \otimes \boldsymbol{n}) \left(\nabla_{\boldsymbol{x}} f + \frac{1}{k_B \theta} m_0 g \boldsymbol{e}_3 f \right)\end{aligned} \tag{2.7}$$

$$\sigma(\boldsymbol{x}, t) = k_B \theta \int_{S^{d-1}} (d\boldsymbol{n} \otimes \boldsymbol{n} - I) \, f(\boldsymbol{x}, t, \boldsymbol{n}) d\boldsymbol{n} \tag{2.8}$$

$$\nabla_{\boldsymbol{x}} \cdot \boldsymbol{u} = 0 \tag{2.9}$$

$$\rho_f \left(\partial_t \boldsymbol{u} + (\boldsymbol{u} \cdot \nabla_{\boldsymbol{x}}) \, \boldsymbol{u} \right) = \mu \Delta_{\boldsymbol{x}} \boldsymbol{u} - \nabla_{\boldsymbol{x}} p + \nabla_{\boldsymbol{x}} \cdot \sigma - \Big(\int_{S^{d-1}} f \, d\boldsymbol{n} \Big) m_0 g \boldsymbol{e}_3 \tag{2.10}$$

2.1. Thermodynamic consistency of the model. To show thermodynamic consistency of the model we use the free energy functional

$$A[f] := \int_\Omega \int_{S^2} (k_B\theta f \ln f + fU(\boldsymbol{x}))\, d\boldsymbol{n}d\boldsymbol{x}, \tag{2.11}$$

where $U(\boldsymbol{x}) = m_0 g\boldsymbol{x}\cdot\boldsymbol{e}_3$ is the gravitational potential.

PROPOSITION 2.1. *For f satisfying the Smoluchowski equation* (2.7)*, the free energy $A[f]$ defined in (2.11) satisfies the identity*

$$\begin{aligned}
&\partial_t A[f] + D_r k_B\theta \int_\Omega\int_{S^2} f|\nabla_{\boldsymbol{n}} \ln f|^2 d\boldsymbol{n}d\boldsymbol{x} \\
&+ D_\perp k_B\theta \int_\Omega\int_{S^2} \nabla_{\boldsymbol{x}}\big(\ln f + \frac{1}{k_B\theta}U\big)\cdot\big(I+\boldsymbol{n}\otimes\boldsymbol{n}\big)\nabla_{\boldsymbol{x}}\big(\ln f + \frac{1}{k_B\theta}U\big) d\boldsymbol{n}d\boldsymbol{x} \\
&= \int_\Omega \nabla_{\boldsymbol{x}}\boldsymbol{u} : \sigma d\boldsymbol{x} + \int_\Omega m_0 g\boldsymbol{e}_3 \left(\int_{S^2} f d\boldsymbol{n}\right)\cdot \boldsymbol{u} d\boldsymbol{x}
\end{aligned} \tag{2.12}$$

Moreover, the total energy

$$E[\boldsymbol{u}, f] = \int_\Omega \left(\frac{1}{2}\rho_f|\boldsymbol{u}|^2 + \int_{S^2}\Big((k_B\theta) f\ln f + fU(\boldsymbol{x})\Big) d\boldsymbol{n}\right) d\boldsymbol{x} \tag{2.13}$$

of the system (2.7)-(2.10) *dissipates.*

The proof is based on vector calculus formulas for the surface gradient operator $\nabla_{\boldsymbol{n}}$. Let $F = F(\boldsymbol{n})$ be a vector valued function and $f = f(\boldsymbol{n})$ be a scalar valued function with $\boldsymbol{n}\in S^{d-1}$. Then the relations

$$\int_{S^2} (\nabla_{\boldsymbol{n}}\cdot F) f d\boldsymbol{n} = -\int_{S^2} F\cdot(\nabla_{\boldsymbol{n}} f - 2\boldsymbol{n} f) d\boldsymbol{n} \tag{2.14}$$

$$\int_{S^2} \boldsymbol{n}\otimes\nabla_{\boldsymbol{n}} f d\boldsymbol{n} = \int_{S^2} \nabla_{\boldsymbol{n}} f\otimes\boldsymbol{n}\, d\boldsymbol{n} = \int_{S^2} (3\boldsymbol{n}\otimes\boldsymbol{n} - \mathrm{id}) f d\boldsymbol{n} \tag{2.15}$$

hold. A proof of (2.14) and (2.15) can be found in an appendix of [23].

Proof: We differentiate (2.11) with respect to t,

$$\partial_t A[f] = \int_\Omega\int_{S^2} \Big(k_B\theta(1+\ln f) + U(\boldsymbol{x})\Big) f_t\, d\boldsymbol{n}d\boldsymbol{x} \tag{2.16}$$

and use (2.7) to express the various contributions.

The contribution of the transport term $-\nabla_{\boldsymbol{x}}\cdot(\boldsymbol{u}f)$ gives

$$\begin{aligned}
I_{tr} &= -\int_\Omega\int_{S^2} \Big(k_B\theta(1+\ln f) + U(\boldsymbol{x})\Big)\nabla_{\boldsymbol{x}}\cdot(\boldsymbol{u}f)\, d\boldsymbol{n}d\boldsymbol{x} \\
&= \int_\Omega\int_{S^2} \Big(k_B\theta\nabla_{\boldsymbol{x}} f + f\nabla_{\boldsymbol{x}} U\Big)\cdot\boldsymbol{u} d\boldsymbol{n}d\boldsymbol{x} \\
&\overset{(2.9)}{=} \int_\Omega m_0 g\boldsymbol{e}_3 \left(\int_{S^2} f d\boldsymbol{n}\right)\cdot\boldsymbol{u}\, d\boldsymbol{x}
\end{aligned}$$

The contribution of the drift term $-\nabla_{\boldsymbol{n}}\cdot(P_{\boldsymbol{n}^\perp}\nabla_{\boldsymbol{x}}\boldsymbol{u}\boldsymbol{n}f)$ is :

$$\begin{aligned}
I_{dr} &= -\int_\Omega\int_{S^2} \Big(k_B\theta(1+\ln f) + U(\boldsymbol{x})\Big)\nabla_{\boldsymbol{n}}\cdot(P_{\boldsymbol{n}^\perp}\nabla_{\boldsymbol{x}}\boldsymbol{u}\boldsymbol{n}f)\, d\boldsymbol{n}d\boldsymbol{x} \\
&\overset{(2.14)}{=} \int_\Omega\int_{S^2} k_B\theta\nabla_{\boldsymbol{n}}\ln f\cdot P_{\boldsymbol{n}^\perp}(\nabla_{\boldsymbol{x}}\boldsymbol{u}\boldsymbol{n}f)\, d\boldsymbol{n}d\boldsymbol{x} \\
&= \int_\Omega \nabla_{\boldsymbol{x}}\boldsymbol{u} : k_B\theta\int_{S^2} \boldsymbol{n}\otimes\nabla_{\boldsymbol{n}} f\, d\boldsymbol{n}\, d\boldsymbol{x} \\
&\overset{(2.15),(2.8)}{=} \int_\Omega \nabla_{\boldsymbol{x}}\boldsymbol{u} : \sigma\, d\boldsymbol{x}.
\end{aligned}$$

The contribution of rotational diffusion leads to

$$\begin{aligned} I_{rd} &= \int_\Omega \int_{S^2} \Big(k_B\theta(1+\ln f) + U(\boldsymbol{x})\Big) D_r \Delta_{\boldsymbol{n}} f \, d\boldsymbol{n} d\boldsymbol{x} \\ &= \int_\Omega \int_{S^2} \Big(k_B\theta(1+\ln f) + U(\boldsymbol{x})\Big) D_r \nabla_{\boldsymbol{n}} \cdot (f \nabla_{\boldsymbol{n}} \ln f) \, d\boldsymbol{n} d\boldsymbol{x} \\ &= -\frac{(k_B\theta)^2}{\zeta_r} \int_\Omega \int_{S^2} |\nabla_{\boldsymbol{n}} \ln f|^2 f \, d\boldsymbol{n} d\boldsymbol{x} \,. \end{aligned}$$

Finally, the contribution of the last term in (2.7), modeling the effect of translational friction and translational diffusion, reads

$$\begin{aligned} I_{tdf} &= \int_\Omega \int_{S^2} \Big(k_B\theta(1+\ln f) + U(\boldsymbol{x})\Big) D_\perp \nabla_{\boldsymbol{x}} \cdot (I + \boldsymbol{n}\otimes\boldsymbol{n}) \left(\nabla_{\boldsymbol{x}} f + \frac{f}{k_B\theta} \nabla_{\boldsymbol{x}} U\right) \\ &= -\frac{(k_B\theta)^2}{\zeta_\perp} \int_{S^2} \int_\Omega \nabla_{\boldsymbol{x}} \left(\ln f + \frac{1}{k_B\theta} U\right) \cdot (I + \boldsymbol{n}\otimes\boldsymbol{n}) f \nabla_{\boldsymbol{x}} \left(\ln f + \frac{1}{k_B\theta} U\right) \end{aligned}$$

Combining all these contributions together yields (2.12).

Next, we multiply the Navier-Stokes equation (2.10) by $\boldsymbol{u}$ and integrate over Ω to obtain the balance of the kinetic energy

$$\begin{aligned} &\frac{d}{dt} \int_\Omega \frac{1}{2} \rho_f |\boldsymbol{u}|^2 d\boldsymbol{x} + \mu \int_\Omega \nabla_{\boldsymbol{x}} \boldsymbol{u} : \nabla_{\boldsymbol{x}} \boldsymbol{u} \, d\boldsymbol{x} \\ &\qquad = -\int_\Omega \nabla_{\boldsymbol{x}} \boldsymbol{u} : \sigma \, d\boldsymbol{x} - \int_\Omega \boldsymbol{u} \cdot m_0 g \boldsymbol{e}_3 \left(\int_{S^2} f d\boldsymbol{n}\right) d\boldsymbol{x} \,. \end{aligned} \tag{2.17}$$

Combining (2.12) and (2.17) leads to the balance of total energy. In particular, it follows that the total energy dissipates.

2.2. Non-dimensionalization. We first list the dimensions of the terms that appear in the equations. The units of mass, length and time are denoted by M, L and T. We also monitor the dependence on the number of particles N.

- v: velocity $\left[\frac{L}{T}\right]$
- $m_0 g$: mass $\times$ acceleration $\left[\frac{ML}{T^2}\right]$;
- $k_B\theta$: energy = force $\times$ length $\left[\frac{ML^2}{T^2}\right]$
- $\zeta_\perp$: translational friction orthogonal to rod = force / velocity $\left[\frac{M}{T}\right]$
  $D_\perp = \frac{k_B\theta}{\zeta_\perp}$ $\left[\frac{L^2}{T}\right]$
- ζ_r: rotational friction = torque / rotational velocity $\left[\frac{ML^2}{T}\right]$
  $D_r = \frac{k_B\theta}{\zeta_r}$ $\left[\frac{1}{T}\right]$
- $\mu = \dfrac{\text{force/area}}{\text{velocity gradient}}$ $\left[\frac{M}{LT}\right]$
- p: pressure = force/area $\left[\frac{M}{LT^2}\right]$
- f: number of particles / volume $\left[\frac{N}{L^3}\right]$
- $\sigma \sim (k_B\theta) f$ $\left[\frac{MN}{LT^2}\right]$

Now we consider a change of scale of the form

$$t = T\hat{t},\ \boldsymbol{x} = X\hat{\boldsymbol{x}},\ \boldsymbol{u} = \frac{X}{T}\hat{\boldsymbol{u}},\ f = \frac{N}{V}\hat{f},\ p = \frac{\mu}{T}\hat{p},\ \sigma = (k_B\theta)\frac{N}{V}\hat{\sigma}. \tag{2.18}$$

In these new units the Smoluchowski equation takes the form

$$\begin{aligned} &\partial_{\hat{t}} \hat{f} + \nabla_{\hat{\boldsymbol{x}}} \cdot \left(\hat{\boldsymbol{u}} \hat{f}\right) + \nabla_{\boldsymbol{n}} \cdot \left(P_{\boldsymbol{n}^\perp} \nabla_{\hat{\boldsymbol{x}}} \hat{\boldsymbol{u}} \boldsymbol{n} \hat{f}\right) = T D_r \Delta_{\boldsymbol{n}} \hat{f} \\ &+ \frac{T}{X^2} D_\perp \nabla_{\hat{\boldsymbol{x}}} \cdot (I + \boldsymbol{n}\otimes\boldsymbol{n}) \nabla_{\hat{\boldsymbol{x}}} \hat{f} + \frac{D_\perp}{X} T \frac{m_0 g}{k_B\theta} \nabla_{\hat{\boldsymbol{x}}} \cdot \left((I + \boldsymbol{n}\otimes\boldsymbol{n}) \boldsymbol{e}_3 \hat{f}\right) \end{aligned} \tag{2.19}$$

The non-dimensionalization of the elastic stress tensor (2.8) leads to the expression

$$\hat{\sigma} = \int_{S^{d-1}} (d\boldsymbol{n} \otimes \boldsymbol{n} - I)\, \hat{f} d\boldsymbol{n}\,, \tag{2.20}$$

while the conservation of momentum for the flow leads to

$$\begin{aligned} &\frac{X^2}{T\mu}\rho_f \left[\partial_{\hat{t}}\hat{\boldsymbol{u}} + (\hat{\boldsymbol{u}}\cdot\nabla_{\hat{\boldsymbol{x}}})\,\hat{\boldsymbol{u}}\right] \\ &= \Delta_{\hat{\boldsymbol{x}}}\hat{\boldsymbol{u}} - \nabla_{\hat{\boldsymbol{x}}}\hat{p} + \frac{XT}{\mu}\frac{k_B\theta}{X}\frac{N}{V}\nabla_{\hat{\boldsymbol{x}}}\cdot\hat{\sigma} - \frac{N}{V}m_0 g\frac{XT}{\mu}\left(\int_{S^{d-1}}\hat{f}\, d\boldsymbol{n}\right)\boldsymbol{e}_3. \end{aligned} \tag{2.21}$$

We have used two length scales in (2.18): a length scale X that is microscopic in nature and a length scale L standing for the size of the macroscopic domain and entering only through the volume V occupied by the suspension $V = O(L^3)$. T is an observational time scale and its role will be clarified later. The ratio X/T is fixed at this point to be the velocity of sedimentation

$$\frac{X}{T} = \frac{m_0 g}{\zeta_\perp} =: v_{sed}, \tag{2.22}$$

i.e. the velocity scale is proportional to the motion of a single rod falling due to gravity in a friction dominated flow.

A review of the Navier-Stokes equation indicates that there are three dimensionless numbers at play: First, a Reynolds number based on the velocity $X/T = v_{sed}$

$$Re := \frac{X v_{sed}}{\frac{\mu}{\rho_f}} = \rho_f \frac{X^2}{T\mu}\,. \tag{2.23}$$

Second, a dimensionless number Γ describing the ratio of elastic versus viscous stresses at the fluid,

$$\begin{aligned} \Gamma := \frac{XT}{\mu}\frac{k_B\theta}{X}\frac{N}{V} &= \left(\frac{X^2\rho_f}{T\mu}\right)\left(\frac{N}{V}\frac{k_B\theta}{\rho_f\left(\frac{X}{T}\right)^2}\right) \\ &= \frac{\text{inertial}}{\text{viscous}}\quad\frac{\text{elastic}}{\text{inertial}} \end{aligned} \tag{2.24}$$

Third, a dimensionless number δ describing the ratio between buoyancy forces and viscous stresses,

$$\begin{aligned} \delta := \frac{N}{V}m_0 g\frac{XT}{\mu} &= \left(\frac{X^2\rho_f}{T\mu}\right)\left(\frac{N m_0 g}{V\rho_f\frac{X}{T^2}}\right) \\ &= \frac{\text{inertial}}{\text{viscous}}\quad\frac{\text{buoyancy}}{\text{inertial}} \end{aligned} \tag{2.25}$$

In interpreting the above definitions one observes that $V\rho_f v_{sed}^2 = V\rho_f\left(\frac{X}{T}\right)^2$ is the total kinetic energy of the sedimenting solution, while $Nk_B\theta$ stands for the total elastic energy of entropic origin of the microstructure. Hence, the last term in (2.24) is the ratio of elastic over inertial forces. The term $V\rho_f\frac{X}{T^2}$ is the inertial force of the solution at the selected length and time scales, while $Nm_0 g$ stands for the total buoyancy force. Hence, the last term in (2.25) stands for the ratio of buoyancy over inertial forces, and in the usual practice of fluid mechanics it will be denoted as $\frac{1}{Fr}$ where Fr is a Froude number. Hence, we have

$$\delta = Re\frac{1}{Fr}$$

We also define

$$\gamma := \frac{\Gamma}{\delta} = \frac{k_B\theta}{Xm_0 g} \tag{2.26}$$

and note that γ stands for the ratio of elastic over buoyancy forces, while δ is the ratio of the buoyancy over viscous stresses. The non-dimensional form of the Navier-Stokes equation then becomes

$$Re\left(\partial_{\hat{t}}\hat{\boldsymbol{u}} + \left(\hat{\boldsymbol{u}}\cdot\nabla_{\hat{\boldsymbol{x}}}\right)\hat{\boldsymbol{u}}\right) = \Delta_{\hat{\boldsymbol{x}}}\hat{\boldsymbol{u}} - \nabla_{\hat{\boldsymbol{x}}}\hat{p} + \delta\gamma\nabla_{\hat{\boldsymbol{x}}}\cdot\sigma - \delta\left(\int_{S^{d-1}}\hat{f}\,d\boldsymbol{n}\right)\boldsymbol{e}_3. \tag{2.27}$$

We turn now to the transport equation (2.19). We introduce the Deborah number

$$De := \frac{1}{D_r T}$$

which as usual expresses the ratio of a stress relaxation time $\frac{1}{D_r}$ over the observational time scale T. We also note that by virtue of (2.26) and (2.22)

$$\frac{T}{X^2}D_\perp\frac{1}{\gamma} = \frac{T}{X^2}\frac{k_B\theta}{\zeta_\perp}\frac{Xm_0g}{k_B\theta} = 1$$

Hence, the kinetic equation (2.19) may be expressed in the dimensionless form

$$\partial_{\hat{t}}\hat{f} + \nabla_{\hat{\boldsymbol{x}}}\cdot\left(\hat{\boldsymbol{u}}\hat{f}\right) + \nabla_{\boldsymbol{n}}\cdot\left(P_{\boldsymbol{n}^\perp}\nabla_{\hat{\boldsymbol{x}}}\hat{\boldsymbol{u}}\boldsymbol{n}\hat{f}\right) = \frac{1}{De}\Delta_{\boldsymbol{n}}\hat{f} + \nabla_{\hat{\boldsymbol{x}}}\cdot\left(I+\boldsymbol{n}\otimes\boldsymbol{n}\right)\left(\gamma\nabla_{\hat{\boldsymbol{x}}}\hat{f} + \boldsymbol{e}_3\hat{f}\right)$$

dependent on two dimensionless numbers: γ defined in (2.26) and the Deborah number De (or equivalently the observational time scale T). In the sequel we will use the notation D_r (of the rotational diffusion coefficient) in the place of $\frac{1}{De}$ in order to simplify the notation.

We summarise the non-dimensional form of the equations (dropping the hats)

$$\begin{aligned}
\partial_t f + \nabla_{\boldsymbol{x}}\cdot(\boldsymbol{u}f) + \nabla_{\boldsymbol{n}}\cdot(P_{\boldsymbol{n}^\perp}\nabla_{\boldsymbol{x}}\boldsymbol{u}\boldsymbol{n}f) - \nabla_{\boldsymbol{x}}\cdot\left(\left(I+\boldsymbol{n}\otimes\boldsymbol{n}\right)\boldsymbol{e}_3 f\right)& \\
= D_r\Delta_{\boldsymbol{n}}f + \gamma\nabla_{\boldsymbol{x}}\cdot\left(I+\boldsymbol{n}\otimes\boldsymbol{n}\right)\nabla_{\boldsymbol{x}}f& \\
\sigma = \int_{S^{d-1}}\left(d\boldsymbol{n}\otimes\boldsymbol{n} - I\right)f\,d\boldsymbol{n}& \\
Re\left(\partial_t\boldsymbol{u} + \left(\boldsymbol{u}\cdot\nabla_{\boldsymbol{x}}\right)\boldsymbol{u}\right) = \Delta_{\boldsymbol{x}}\boldsymbol{u} - \nabla_{\boldsymbol{x}}p + \delta\gamma\nabla_{\boldsymbol{x}}\cdot\sigma - \delta\left(\int_{S^{d-1}}f\,d\boldsymbol{n}\right)\boldsymbol{e}_3& \\
\nabla_{\boldsymbol{x}}\cdot\boldsymbol{u} = 0&
\end{aligned} \tag{2.28}$$

If we express the Navier-Stokes equation in the equivalent form (2.6), then the associated non-dimensional form is given by

$$\begin{aligned}
Re\left(\partial_t\boldsymbol{u} + \left(\boldsymbol{u}\cdot\nabla_{\boldsymbol{x}}\right)\boldsymbol{u}\right) = \Delta_{\boldsymbol{x}}\boldsymbol{u} - \nabla_{\boldsymbol{x}}p + \delta\gamma\nabla_{\boldsymbol{x}}\cdot\sigma + \delta\left(1 - \int_{S^{d-1}}f\,d\boldsymbol{n}\right)\boldsymbol{e}_3& \\
\nabla_{\boldsymbol{x}}\cdot\boldsymbol{u} = 0&
\end{aligned} \tag{2.29}$$

2.3. Multi-scale mechanism for instability and cluster formation. The multi-scale mechanism that leads to the instability and the formation of clusters was first explained by Koch and Shaqfeh, see [19].

In our kinetic model, the function

$$\rho(\boldsymbol{x},t) = \int_{S^{d-1}}f(\boldsymbol{x},t,\boldsymbol{n})d\boldsymbol{n}$$

measures the density of rod like particles. By virtue of the buoyancy term in the Stokes equation, a density modulation (as indicated in Figure 2.2 (a)) triggers a modulated shear flow with flow direction $\boldsymbol{e}_3$ (see Fig. 2.2 (b)).

By virtue of the microscopic drift term on the sphere $\nabla_{\boldsymbol{n}}\cdot(P_{\boldsymbol{n}^\perp}\nabla_{\boldsymbol{x}}\boldsymbol{u}\boldsymbol{n}f)$ this shear destroys the uniform distribution f in $\boldsymbol{n}$. For moderate local Deborah numbers the distribution f slightly concentrates in a direction at 45 degrees between the flow direction and the shear direction as shown in Fig. 2.2 (c). For larger shear rates the distribution f concentrates more pronounced in direction of gravity.

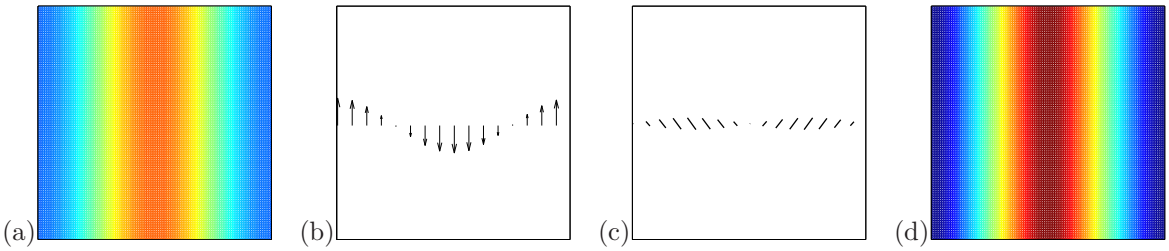

FIG. 2.2. *Illustration of the concentration mechanism (a) initial density modulation, (b) velocity field, (c) microscopic orientation: plot of $\lambda \boldsymbol{r}$, where λ is the largest eigenvalue of σ and $\boldsymbol{r}$ is the corresponding eigenvector, (d) increased density modulation at later time.*

In this figure we plotted the average microscopic orientation $\lambda \boldsymbol{r}$, where λ is the largest eigenvalue of σ and $\boldsymbol{r}$ is the corresponding eigenvector.

By virtue of the term $-\nabla_{\boldsymbol{x}} \cdot ((I + \boldsymbol{n} \otimes \boldsymbol{n})\, \boldsymbol{e}_3 f)$ this nonuniform distribution in $\boldsymbol{n}$ implies that particles on average fall in a direction which is at a non-vanishing angle between flow direction and shear direction. Hence this term acts as a horizontal drift term for the modulated density ρ . In fact, it reinforces the original horizontal modulation of the density ρ since particles with an orientation as shown in Fig. 2.2 (c) move towards the center.

The goal of this article is to provide a quantitative analysis of the mechanism of cluster formation. In the process we will use the model (2.28) as well as some simplified problems derived from that system.

2.4. Perturbation of the quiescent flow - the linearized problem. The problem (2.28) admits a special class of trivial solutions describing a quiescent flow. One verifies that functions $(\bar{f}, \bar{u}, \bar{\sigma}, \bar{p})$ given by

$$\bar{f} = f_0\,, \quad \bar{u} = 0\,, \quad \bar{\sigma} = \sigma_0\,, \quad \bar{p} = p_0(x) = -\delta f_0 a_{d-1} \boldsymbol{e}_3 \cdot \boldsymbol{x} \tag{2.30}$$

where f_0 is a constant,

$$\sigma_0 := f_0 \int_{S^{d-1}} (d\boldsymbol{n} \otimes \boldsymbol{n} - I)\, d\boldsymbol{n}\,,$$

and $a_{d-1} = \int_{S^{d-1}} 1 d\boldsymbol{n}$ the area of the (d-1)-dimensional sphere, are special solutions for any constant f_0, where $p_0(x)$ stands for hydrostatic pressure induced by the presence of the rods.

We derive now the linearized equation obeyed for a perturbation of the quiescent flow. For simplicity take $f_0 = 1$, that is the basic flow is $\bar{f} = 1$, $\bar{u} = 0$, $\bar{p} = p_0(x) = -\delta a_{d-1} \boldsymbol{e}_3 \cdot \boldsymbol{x}$. Write

$$f = 1 + F\,, \quad u\,, \quad \sigma = \sigma_0 + \Sigma\,, \quad p = p_0(x) + P \tag{2.31}$$

a perturbation of the flow and let

$$m = \int \int_{S^{d-1}} F(\boldsymbol{x}, \boldsymbol{n}) d\boldsymbol{n} d\boldsymbol{x}$$

be the initial mass of the perturbation (which is of course conserved).

One computes easily that the linearized system satisfied by the perturbation (F, u, P) of the flow is

$$\begin{aligned} \partial_t F + \nabla_{\boldsymbol{n}} \cdot (P_{\boldsymbol{n}^\perp} \nabla_{\boldsymbol{x}} \boldsymbol{u} \boldsymbol{n}) - \nabla_{\boldsymbol{x}} \cdot ((I + \boldsymbol{n} \otimes \boldsymbol{n})\, \boldsymbol{e}_3 F) &= D_r \Delta_{\boldsymbol{n}} F + \gamma \nabla_{\boldsymbol{x}} \cdot (I + \boldsymbol{n} \otimes \boldsymbol{n})\, \nabla_{\boldsymbol{x}} F \\ \Sigma &= \int_{S^{d-1}} (d\boldsymbol{n} \otimes \boldsymbol{n} - I)\, F\, d\boldsymbol{n} \\ Re \partial_t \boldsymbol{u} = \Delta_{\boldsymbol{x}} \boldsymbol{u} - \nabla_{\boldsymbol{x}} (P + \delta m \boldsymbol{e}_3 \cdot \boldsymbol{x}) + \delta \gamma \nabla_{\boldsymbol{x}} \cdot \Sigma + \delta \big(m - \int_{S^{d-1}} F\, d\boldsymbol{n}\big) \boldsymbol{e}_3 \\ \nabla_{\boldsymbol{x}} \cdot \boldsymbol{u} = 0 \end{aligned} \tag{2.32}$$

The study of the linearized system (2.32) is a challenging problem, even if one restricts to the case $\gamma = 0$ where the elastic effects of the microstructure decouple. Nevertheless, it is an important problem

for the following reason: Statistical analysis of realisations of sedimenting flows in the experimental works [13, 14] indicates that there exists a characteristic length associated to the cluster formation. It would be important to study if the linearized analysis can predict such a length selection mechanism and how it relates to the various parameters of the flow. We have taken a step in this direction in Appendix B: for a linearized moment closure approximation of shear flow, we perform a linear stability analysis and show that when $Re > 0$ then there exists a most unstable wavelength.

2.5. Some special sedimenting flows. We now present some special flows that are adapted to sedimentation of rigid rods in the vertical direction. The flows take place in $\mathbb{R}^3$ with the generic point $\boldsymbol{x} = (x, y, z)^T$. The gravity is in the direction of the negative z-axis, while the rigid rods take values on the sphere $\boldsymbol{n} = (n_1, n_2, n_3)^T \in S^2$.

2.5.1. Rectilinear flows. We consider first the question whether (2.28) admits solutions following the *ansatz* of a rectilinear flow, namely

$$f = f(t, x, y, \boldsymbol{n}), \quad \boldsymbol{u} = \begin{pmatrix} u \\ v \\ w \end{pmatrix} = \begin{pmatrix} 0 \\ 0 \\ w(t, x, y) \end{pmatrix}, \quad p = p(t, x, y, z). \tag{2.33}$$

The incompressibility condition is automatically satisfied, equation $(2.28)_1$ gives

$$\begin{aligned} &\partial_t f + \nabla_{\boldsymbol{n}} \cdot \left[P_{\boldsymbol{n}^\perp}(0, 0, n_1 \partial_x w + n_2 \partial_y w)^T f \right] - \partial_x(n_1 n_3 f) - \partial_y(n_2 n_3 f) \\ &\quad = D_r \Delta_{\boldsymbol{n}} f + \gamma \Big((1 + n_1^2)\partial_x^2 f + 2 n_1 n_2 \partial_x \partial_y f + (1 + n_2^2)\partial_y^2 f \Big), \end{aligned} \tag{2.34}$$

while the Navier-Stokes equation $(2.28)_3$ reduces to

$$\begin{aligned} \partial_x p &= \delta\gamma(\partial_x \sigma_{11} + \partial_y \sigma_{12}) \\ \partial_y p &= \delta\gamma(\partial_x \sigma_{21} + \partial_y \sigma_{22}) \\ \partial_z p &= -Re \, \frac{\partial w}{\partial t} + \triangle_{(x,y)} w + \delta\gamma(\partial_x \sigma_{31} + \partial_y \sigma_{32}) - \delta \int_{S^2} f \, d\boldsymbol{n} \end{aligned} \tag{2.35}$$

where $\triangle_{(x,y)}$ stands for the two-dimensional Laplace operator and

$$\sigma = \sigma(t, x, y) = \int_{S^2} (3\boldsymbol{n} \otimes \boldsymbol{n} - I) \, f \, d\boldsymbol{n}. \tag{2.36}$$

The ansatz (2.33) implies the right hand side in $(2.35)_3$ depends only on (x, y). We deduce that the pressure

$$p = \kappa z + P(x, y),$$

where κ is arbitrary and reflects the effect of an imposed pressure gradient (or it might even be that $\kappa = \kappa(t)$ if the imposed gradient varies with time). The functions (f, w) are selected by solving the coupled system consisting of (2.34), (2.36) and

$$Re \, \frac{\partial w}{\partial t} = \triangle_{(x,y)} w + \delta\gamma(\partial_x \sigma_{31} + \partial_y \sigma_{32}) + \delta(m - \int_{S^2} f \, d\boldsymbol{n}). \tag{2.37}$$

In (2.37) we selected the constant $\kappa = \partial_z p = -\delta m$ with m the total mass

$$m = \iint \int_{S^2} f \, d\boldsymbol{n} \, dx \, dy$$

which is conserved under appropriate (say periodic) boundary conditions in (x, y). Note that there is an arbitrary gradient of pressure that can be imposed from the outside. The selected constant is the one amounting to equilibration of the mean flow.

Finally, in order to understand the solution of (2.34), (2.36), (2.37) as a rectilinear flow we have to select the pressure $P(x,y)$ by solving

$$\begin{aligned}\partial_x P &= \delta\gamma(\partial_x\sigma_{11} + \partial_y\sigma_{12})\\ \partial_y P &= \delta\gamma(\partial_x\sigma_{21} + \partial_y\sigma_{22})\end{aligned} \tag{2.38}$$

This system is consistent provided that σ satisfies the consistency condition

$$\partial_{xy}(\sigma_{11} - \sigma_{22}) + (\partial_{yy} - \partial_{xx})\sigma_{12} = 0\,.$$

Such conditions reflect symmetries of the initial data that give rise to the special rectilinear flow and will not be pursued further here. In the sequel, we only consider the special case $\gamma = 0$ reflecting the case that elastic forces are much less important than buoyancy forces. This also has the effect that translational Brownian motion is neglected. For the case $\gamma = 0$ we have $P(x,y) = const$ and the pressure takes the form $p = -mz$.

2.5.2. Shear flows. Shear flows follow the ansatz

$$f = f(t,x,\boldsymbol{n})\,, \quad \boldsymbol{u} = \begin{pmatrix} 0\\ 0\\ w(t,x)\end{pmatrix}\,, \quad p = p(t,x,z)\,. \tag{2.39}$$

where x is the horizontal direction and z is the vertical direction (as before). However, $\boldsymbol{n}$ is still allowed to take values in S^2 which means that the rigid rods are allowed to move out of the plane of the shear flow. Shear flow is a special case of the rectilinear flow, and adapting the equations from the previous section we conclude that (f,w) satisfy the coupled system

$$\begin{aligned}\partial_t f + \nabla_{\boldsymbol{n}}\cdot\left[P_{\boldsymbol{n}^\perp}(0,0,n_1\partial_x w)^T f\right] - \partial_x(n_1 n_3 f) &= D_r\Delta_{\boldsymbol{n}} f + \gamma(1+n_1^2)\partial_x^2 f\\ Re\,\frac{\partial w}{\partial t} &= \partial_x^2 w + \delta\gamma\partial_x\sigma_{31} + \delta\Big(m - \int_{S^2} f\,d\boldsymbol{n}\Big)\end{aligned} \tag{2.40}$$

3. Derivation of a nonlinear moment closure. Henceforth we take for simplicity $D_r = 1$ and consider the Smoluchowski equation in the form

$$\begin{aligned}&\partial_t f + \nabla_{\boldsymbol{x}}\cdot(\boldsymbol{u}f) + \nabla_{\boldsymbol{n}}\cdot(P_{\boldsymbol{n}^\perp}\nabla_{\boldsymbol{x}}\boldsymbol{u}\boldsymbol{n}f)\\ &\quad = \Delta_{\boldsymbol{n}} f + \gamma\nabla_{\boldsymbol{x}}\cdot(I + \boldsymbol{n}\otimes\boldsymbol{n})\,\nabla_{\boldsymbol{x}} f + \nabla_{\boldsymbol{x}}\cdot((I+\boldsymbol{n}\otimes\boldsymbol{n})\,f\boldsymbol{e}_3)\end{aligned} \tag{3.1}$$

3.1. Equations of moments. The objective is to derive a moment system at the level of second moments. We define the quantities:

$$\begin{aligned}0^{th}\text{ moment:}&\qquad \rho := \int_{S^{d-1}} f d\boldsymbol{n}\\ 2^{nd}\text{moment:}&\quad S := \int_{s^{d-1}}\left(\boldsymbol{n}\otimes\boldsymbol{n} - \frac{1}{d}I\right) f d\boldsymbol{n}, \quad i.e.\ S_{ij} = \int_{S^{d-1}}\left(n_i n_j - \frac{1}{d}\delta_{ij}\right) f d\boldsymbol{n}\\ 4^{th}\text{moment:}&\quad P := \int_{S^{d-1}} \boldsymbol{n}\otimes\boldsymbol{n}\otimes\boldsymbol{n}\otimes\boldsymbol{n} f d\boldsymbol{n}, \quad i.e.\ P_{\alpha\beta ij} = \int_{S^{d-1}} n_\alpha n_\beta n_i n_j f d\boldsymbol{n}\end{aligned}$$

The evolution equation for ρ is obtained by integrating the Smoluchowski equation (3.1) over the sphere S^{d-1}. There are no contributions from the third and fourth term, and we obtain

$$\begin{aligned}\partial_t\rho + \boldsymbol{u}\cdot\nabla_{\boldsymbol{x}}\rho &= \gamma\nabla_{\boldsymbol{x}}\cdot\int_{S^{d-1}}(I+\boldsymbol{n}\otimes\boldsymbol{n})\,\nabla_{\boldsymbol{x}} f d\boldsymbol{n} + \nabla_{\boldsymbol{x}}\cdot\int_{S^{d-1}}(I+\boldsymbol{n}\otimes\boldsymbol{n})\,f\boldsymbol{e}_3 d\boldsymbol{n}\\ &= \gamma\nabla_{\boldsymbol{x}}\cdot\nabla_{\boldsymbol{x}}\cdot\int_{S^{d-1}}\left(\left(\boldsymbol{n}\otimes\boldsymbol{n} - \frac{1}{d}I\right) + \frac{d+1}{d}I\right) f d\boldsymbol{n}\\ &\qquad + \nabla_{\boldsymbol{x}}\cdot\int_{S^{d-1}}\left(\left(\boldsymbol{n}\otimes\boldsymbol{n} - \frac{1}{d}I\right) + \frac{d+1}{d}I\right)\boldsymbol{e}_3 f d\boldsymbol{n}\\ &= \gamma\nabla_{\boldsymbol{x}}\cdot\nabla_{\boldsymbol{x}}\cdot\left(S + \frac{d+1}{d}I\rho\right) + \nabla_{\boldsymbol{x}}\cdot\left[\left(S + \frac{d+1}{d}I\rho\right)\boldsymbol{e}_3\right]\end{aligned}$$

Next we derive the evolution equation for the components of S. Note that in the following we make frequent use of the Einstein summation convention. Multiplying (3.1) with $\left(\boldsymbol{n}\otimes\boldsymbol{n}-\frac{1}{d}I\right)$ and integrating over S^{d-1}, provides

$$\begin{aligned}
&\partial_t S_{\alpha\beta}+(\boldsymbol{u}\cdot\nabla_{\boldsymbol{x}})\,S_{\alpha\beta}+\underbrace{\int_{S^{d-1}}\left(n_\alpha n_\beta-\frac{1}{d}\delta_{\alpha\beta}\right)\nabla_{\boldsymbol{n}}\cdot\left(P_{\boldsymbol{n}^\perp}\nabla_{\boldsymbol{x}}\boldsymbol{u}\boldsymbol{n}f\right)d\boldsymbol{n}}_{(I_1)_{\alpha\beta}}\\
&\quad=\underbrace{\int_{S^{d-1}}\left(n_\alpha n_\beta-\frac{1}{d}\delta_{\alpha\beta}\right)\Delta_{\boldsymbol{n}}f d\boldsymbol{n}}_{(I_2)_{\alpha\beta}}+\gamma\underbrace{\int_{S^{d-1}}\left(n_\alpha n_\beta-\frac{1}{d}\delta_{\alpha\beta}\right)\nabla_{\boldsymbol{x}}\cdot\left(I+\boldsymbol{n}\otimes\boldsymbol{n}\right)\nabla_{\boldsymbol{x}}f d\boldsymbol{n}}_{(I_3)_{\alpha\beta}}\\
&\quad+\underbrace{\int_{S^{d-1}}\left(n_\alpha n_\beta-\frac{1}{d}\delta_{\alpha\beta}\right)\nabla_{\boldsymbol{x}}\cdot\left(I+\boldsymbol{n}\otimes\boldsymbol{n}\right)f\boldsymbol{e}_3 d\boldsymbol{n}}_{(I_4)_{\alpha\beta}}.
\end{aligned}$$

We now calculate the different integrals separately.

$$\begin{aligned}
I_1&=\int_{S^{d-1}}\left(\boldsymbol{n}\otimes\boldsymbol{n}-\frac{1}{d}I\right)\nabla_{\boldsymbol{n}}\cdot P_{\boldsymbol{n}^\perp}\nabla_{\boldsymbol{x}}\boldsymbol{u}\boldsymbol{n}f d\boldsymbol{n}=-\int_{S^{d-1}}\nabla_{\boldsymbol{n}}\left(\boldsymbol{n}\otimes\boldsymbol{n}-\frac{1}{d}I\right)\cdot P_{\boldsymbol{n}^\perp}\nabla_{\boldsymbol{x}}\boldsymbol{u}\boldsymbol{n}f d\boldsymbol{n}\\
&=-\underbrace{\int_{S^{d-1}}\nabla_{\boldsymbol{n}}\left(\boldsymbol{n}\otimes\boldsymbol{n}\right)\cdot\nabla_{\boldsymbol{x}}\boldsymbol{u}\boldsymbol{n}f d\boldsymbol{n}}_{I_1^1}+\underbrace{\int_{S^{d-1}}\boldsymbol{n}\left(\left(\boldsymbol{n}\cdot\nabla_{\boldsymbol{n}}\right)\boldsymbol{n}\otimes\boldsymbol{n}\right)\cdot\nabla_{\boldsymbol{x}}\boldsymbol{u}\boldsymbol{n}f d\boldsymbol{n}}_{I_1^2}
\end{aligned}$$

where

$$\begin{aligned}
(I_1^1)_{\alpha\beta}&=\int_{S^{d-1}}\nabla_{\boldsymbol{n}}\left(n_\alpha n_\beta\right)\cdot\nabla_{\boldsymbol{x}}\boldsymbol{u}\boldsymbol{n}f d\boldsymbol{n}=\int_{S^{d-1}}\frac{\partial}{\partial n_i}\left(n_\alpha n_\beta\right)\frac{\partial u_i}{\partial x_j}n_j f d\boldsymbol{n}\\
&=\int_{S^{d-1}}\left(\delta_{i\alpha}n_\beta+n_\alpha\delta_{i\beta}\right)\frac{\partial u_i}{\partial x_j}n_j f d\boldsymbol{n}=\int_{S^{d-1}}\frac{\partial u_\alpha}{\partial x_j}n_j n_\beta f+\frac{\partial u_\beta}{\partial x_j}n_\alpha n_j f d\boldsymbol{n}\\
&=\int_{S^{d-1}}\left(\frac{\partial u_\alpha}{\partial x_j}\left(n_j n_\beta-\frac{1}{d}\delta_{j\beta}\right)+\frac{\partial u_\beta}{\partial x_j}\left(n_\alpha n_j-\frac{1}{d}\delta_{\alpha j}\right)+\frac{1}{d}\left(\frac{\partial u_\alpha}{\partial x_\beta}+\frac{\partial u_\beta}{\partial x_\alpha}\right)\right)f d\boldsymbol{n}\\
&=\frac{\partial u_\alpha}{\partial x_j}S_{j\beta}+\frac{\partial u_\beta}{\partial x_j}S_{\alpha j}+\frac{1}{d}\left(\frac{\partial u_\alpha}{\partial x_\beta}+\frac{\partial u_\beta}{\partial x_\alpha}\right)\rho
\end{aligned}$$

i.e.

$$I_1^1=\nabla_{\boldsymbol{x}}\boldsymbol{u}S+S\nabla_{\boldsymbol{x}}\boldsymbol{u}^T+\frac{1}{d}\left(\nabla_{\boldsymbol{x}}\boldsymbol{u}+\nabla_{\boldsymbol{x}}\boldsymbol{u}^T\right)\rho,$$

and

$$\begin{aligned}
(I_1^2)_{\alpha\beta}&=\int_{S^{d-1}}n_k\frac{\partial}{\partial n_k}\left(n_\alpha n_\beta\right)n_i\frac{\partial u_i}{\partial x_j}n_j f d\boldsymbol{n}=\int_{S^{d-1}}n_k\left(\delta_{\alpha k}n_\beta+n_\alpha\delta_{k\beta}\right)n_i\frac{u_i}{\partial x_j}n_j f d\boldsymbol{n}\\
&=2\frac{\partial u_i}{\partial x_j}\int_{S^{d-1}}n_\alpha n_\beta n_i n_j f d\boldsymbol{n}
\end{aligned}$$

i.e.

$$I_1^2=2P:\nabla_{\boldsymbol{x}}\boldsymbol{u}.$$

Therefore,

$$I_1=-\nabla_{\boldsymbol{x}}\boldsymbol{u}S-S\nabla_{\boldsymbol{x}}\boldsymbol{u}^T-\frac{1}{d}\left(\nabla_{\boldsymbol{x}}\boldsymbol{u}+\nabla_{\boldsymbol{x}}\boldsymbol{u}^T\right)\rho+2P:\nabla_{\boldsymbol{x}}\boldsymbol{u}.$$

We next turn to I_2:

$$\begin{aligned} I_2 &= \int_{S^{d-1}} \left(\boldsymbol{n} \otimes \boldsymbol{n} - \frac{1}{d} I \right) \Delta_{\boldsymbol{n}} f d\boldsymbol{n} \\ &= \int_{S^{d-1}} \Delta_{\boldsymbol{n}} \left(\boldsymbol{n} \otimes \boldsymbol{n} - \frac{1}{d} I \right) f d\boldsymbol{n} \\ &= 2d \int_{S^{d-1}} \left(\boldsymbol{n} \otimes \boldsymbol{n} - \frac{1}{d} I \right) f d\boldsymbol{n} = 2dS \end{aligned}$$

Note that the components of S are the surface spherical harmonics of order 2 and thus eigenfunctions of the Laplacian on S.

For I_3 and I_4 we obtain

$$(I_3)_{\alpha\beta} = \partial_{x_i} \partial_{x_j} \left(S_{\alpha\beta}\delta_{ij} + P_{\alpha\beta ij} - \frac{1}{d}\delta_{\alpha\beta} S_{ij} + \frac{1}{d^2}\delta_{\alpha\beta}\delta_{ij}\rho \right)$$

$$(I_4)_{\alpha\beta} = \partial_{x_i} \Big(P_{\alpha\beta i3} - \frac{1}{d}\delta_{\alpha\beta} S_{i3} + \frac{1}{d^2}\delta_{\alpha\beta}\delta_{i3}\rho + S_{\alpha\beta}\delta_{i3} \Big)$$

Putting these together, we obtain evolution equations for ρ and S:

$$\begin{aligned} &\partial_t \rho + \boldsymbol{u} \cdot \nabla_{\boldsymbol{x}} \rho = \gamma \nabla_{\boldsymbol{x}} \cdot \nabla_{\boldsymbol{x}} \cdot \left(S + \frac{d+1}{d} \rho I \right) + \nabla_{\boldsymbol{x}} \cdot \left(S + \frac{d+1}{d} \rho I \right) \boldsymbol{e}_3 \\ &\partial_t S_{\alpha\beta} + (\boldsymbol{u} \cdot \nabla_{\boldsymbol{x}}) S_{\alpha\beta} - \frac{\partial u_\alpha}{\partial_{x_j}} S_{j\beta} - \frac{\partial u_\beta}{\partial x_j} S_{\alpha j} - \frac{1}{d} \left(\frac{\partial u_\alpha}{\partial x_\beta} + \frac{\partial u_\beta}{\partial x_\alpha} \right) \rho + 2 P_{\alpha\beta ij} \frac{\partial u_i}{\partial x_j} \\ &\quad = -2dS_{\alpha\beta} + \gamma \partial_{x_i} \partial_{x_j} \left(S_{\alpha\beta}\delta_{ij} + P_{\alpha\beta ij} - \frac{1}{d}\delta_{\alpha\beta} S_{ij} + \frac{1}{d^2}\delta_{\alpha\beta}\delta_{ij}\rho \right) \\ &\quad + \partial_{x_i} \left(P_{\alpha\beta i3} - \frac{1}{d}\delta_{\alpha\beta} S_{i3} + \frac{1}{d^2}\delta_{\alpha\beta}\delta_{i3}\rho + S_{\alpha\beta}\delta_{i3} \right) \end{aligned} \tag{3.2}$$

3.2. Moment closure. The evolution equation for ρ is expressed in terms of 0^{th} and 2^{nd} moments, the evolution equation of S involves 2^{nd} and 4^{th}-order moments and so on. We would like to close the system at the level of the 2^{nd}-order moments.

The problem of moment closure is studied in detail in [16] for a related (but simpler) problem of a suspension of rigid particles subjected to a homogeneous time-dependent flow with constant strain rate. The kinetic equation used in [16] is a Fokker-Planck type equation, depending on the microscopic orientation. For our model we would obtain a similar kinetic equation if we restrict our considerations to a constant externally imposed velocity gradient. Various methodologies of closure are proposed mostly based on approximating limiting equilibrium flows. The reader is referred to [15, 16] and [5, Sec 8.6.2] for a discussion of various closure mechanisms.

In the present problem, the kinetic function depends both on the kinetic and the spatial variable and is expected to have different behaviors in different regions of the flow domain: the microstructure is expected to be strongly oriented inside the clusters but nearly isotropic in regions away from the clusters. We thus will perform a closure that is not associated to an expected Maxwellian, but rather uses the geometric structure of harmonic polynomials outlined in Appendix A, in particular (A.2). We will close the system at the level of second moments by projecting the fourth order homogeneous polynomials to the subspace of spherical harmonics of 2^{nd} and 0^{th}-order. This has the advantage that it is a general rule equally applicable to the whole flow region, but the disadvantage that its validity cannot be quantitatively assessed via an asymptotic method. To carry out the procedure, we employ (A.2) and express the higher order terms of $P_{\alpha\beta ij}$ in terms of the harmonic polynomial basis presented in Appendix A. To get a moment closure on the level of second moments, we then neglect all the projections to the 4^{th} order part of the basis and retain only the projections to the 2^{nd} and 0^{th}-order part of the basis.

In the sequel we restrict to special flows, shear or rectilinear flows, and implement this derivation in Sections 3.3 and 3.4. For these special flows, the only terms of the form $P_{\alpha\beta ij}$ which do not cancel are $P_{\alpha\beta 13} = P_{\alpha\beta 31}$ and $P_{\alpha\beta 23} = P_{\alpha\beta 32}$. We restrict our considerations to these terms, and introduce the notations $p_{\alpha\beta ij} = n_\alpha n_\beta n_i n_j$ and the matrix s with entries $s_{ij} = n_i n_j - \frac{1}{3}\delta_{ij}$, $i, j = 1, 2, 3$. Note that

$$s = \begin{pmatrix} n_1^2 - \frac{1}{3} & n_1 n_2 & n_1 n_3 \\ \cdot & n_2^2 - \frac{1}{3} & n_2 n_3 \\ \cdot & \cdot & n_3^2 - \frac{1}{3} \end{pmatrix} = \begin{pmatrix} \frac{1}{2}P_2^{-2} - \frac{1}{2}P_2^0 & \frac{1}{2}P_2^2 & P_2^{-1} \\ \cdot & -\frac{1}{2}P_2^{-2} - \frac{1}{2}P_2^0 & P_2^1 \\ \cdot & \cdot & P_2^0 \end{pmatrix},$$

where we used the harmonic polynomial basis of Appendix A and only write out the upper part of the symmetric matrix.

Now we can verify that

$$(p_{\alpha\beta 13})_{\alpha,\beta=1,2,3} = \begin{pmatrix} n_1^3 n_3 & n_1^2 n_2 n_3 & n_1^2 n_3^2 \\ \cdot & n_1 n_2^2 n_3 & n_1 n_2 n_3^2 \\ \cdot & \cdot & n_1 n_3^3 \end{pmatrix}$$

$$= \begin{pmatrix} \sin^3\theta\cos\theta\cos^3\phi & \sin^3\theta\cos\theta\sin\phi\cos^2\phi & \sin^2\theta\cos^2\theta\cos^2\phi \\ \cdot & \sin^3\theta\cos\theta\sin^2\phi\cos\phi & \sin^2\theta\cos^2\theta\sin\phi\cos\phi \\ \cdot & \cdot & \sin\theta\cos^3\theta\cos\phi \end{pmatrix}$$

$$= \begin{pmatrix} \frac{1}{4}P_4^{-3} - \frac{3}{28}P_4^{-1} + \frac{3}{7}s_{13} & \frac{1}{4}P_4^3 - \frac{1}{28}P_4^1 + \frac{1}{7}s_{23} & \frac{1}{14}P_4^{-2} - \frac{1}{70}P_4^0 - \frac{1}{7}s_{22} + \frac{1}{15} \\ \cdot & -\frac{1}{4}P_4^{-3} - \frac{1}{28}P_4^{-1} + \frac{1}{7}s_{13} & \frac{1}{14}P_4^2 + \frac{1}{7}s_{12} \\ \cdot & \cdot & \frac{1}{7}P_4^{-1} + \frac{3}{7}s_{13} \end{pmatrix}$$

and

$$(p_{\alpha\beta 23})_{\alpha,\beta=1,2,3} = \begin{pmatrix} n_1^2 n_2 n_3 & n_1 n_2^2 n_3 & n_1 n_2 n_3^2 \\ \cdot & n_2^3 n_3 & n_2^2 n_3^2 \\ \cdot & \cdot & n_2 n_3^3 \end{pmatrix}$$

$$= \begin{pmatrix} \sin^3\theta\cos\theta\sin\phi\cos^2\phi & \sin^3\theta\cos\theta\sin^2\phi\cos\phi & \sin^2\theta\cos^2\theta\sin\phi\cos\phi \\ \cdot & \sin^3\theta\cos\theta\sin^3\phi & \sin^2\theta\cos^2\theta\sin^2\phi \\ \cdot & \cdot & \sin\theta\cos^3\theta\sin\phi \end{pmatrix}$$

$$= \begin{pmatrix} \frac{1}{4}P_4^3 - \frac{1}{28}P_4^1 + \frac{1}{7}s_{23} & -\frac{1}{4}P_4^{-3} - \frac{1}{28}P_4^{-1} + \frac{1}{7}s_{13} & \frac{1}{14}P_4^2 + \frac{1}{7}s_{12} \\ \cdot & -\frac{1}{4}P_4^3 - \frac{3}{28}P_4^1 + \frac{3}{7}s_{23} & -\frac{1}{14}P_4^{-2} - \frac{1}{70}P_4^0 - \frac{1}{7}s_{11} + \frac{1}{15} \\ \cdot & \cdot & \frac{1}{7}P_4^1 + \frac{3}{7}s_{23} \end{pmatrix}.$$

Finally we drop higher order terms, i.e. we drop all the multiples of the 4th order basis polynomials, and obtain the approximations

$$(p_{\alpha\beta 13})_{\alpha,\beta=1,2,3} \approx \begin{pmatrix} \frac{3}{7}s_{13} & \frac{1}{7}s_{23} & -\frac{1}{7}s_{22} + \frac{1}{15} \\ \cdot & \frac{1}{7}s_{13} & \frac{1}{7}s_{12} \\ \cdot & \cdot & \frac{3}{7}s_{13} \end{pmatrix}$$

$$(p_{\alpha\beta 23})_{\alpha,\beta=1,2,3} \approx \begin{pmatrix} \frac{1}{7}s_{23} & \frac{1}{7}s_{13} & \frac{1}{7}s_{12} \\ \cdot & \frac{3}{7}s_{23} & -\frac{1}{7}s_{11} + \frac{1}{15} \\ \cdot & \cdot & \frac{3}{7}s_{23} \end{pmatrix}.$$

Now it is straight forward to see that $P_{\alpha\beta 13}$ and $P_{\alpha\beta 23}$ can analogously be approximated by

$$\begin{aligned}(P_{\alpha\beta 13})_{\alpha,\beta=1,2,3} &\approx \begin{pmatrix} \frac{3}{7}S_{13} & \frac{1}{7}S_{23} & -\frac{1}{7}S_{22}+\frac{1}{15}\rho \\ \cdot & \frac{1}{7}S_{13} & \frac{1}{7}S_{12} \\ \cdot & \cdot & \frac{3}{7}S_{13} \end{pmatrix} \\ (P_{\alpha\beta 23})_{\alpha,\beta=1,2,3} &\approx \begin{pmatrix} \frac{1}{7}S_{23} & \frac{1}{7}S_{13} & \frac{1}{7}S_{12} \\ \cdot & \frac{3}{7}S_{23} & -\frac{1}{7}S_{11}+\frac{1}{15}\rho \\ \cdot & \cdot & \frac{3}{7}S_{23} \end{pmatrix}. \end{aligned} \tag{3.3}$$

Furthermore, we note that $P_{\alpha\beta 13} = P_{\alpha\beta 31}$ and $P_{\alpha\beta 23} = P_{\alpha\beta 32}$ holds for all $\alpha, \beta = 1, 2, 3$.

3.3. Shear flow. In the special case of shear flow, we consider functions of the form

$$\begin{aligned} f &= f(t, x, \boldsymbol{n}) \\ \boldsymbol{u} &= (0, 0, w(t, x))^T \\ S_{ij} &= S_{ij}(t, x). \end{aligned} \tag{3.4}$$

Furthermore, we restrict our considerations to the case $\gamma = 0$. Under these assumptions, the system (3.2) can be written in the form

$$\begin{aligned} \partial_t \rho &= \partial_x S_{13} \\ \partial_t S_{\alpha\beta} - \frac{\partial u_\alpha}{\partial x} S_{1\beta} - \frac{\partial u_\beta}{\partial x} S_{\alpha 1} - \frac{1}{d}\left(\frac{\partial u_\alpha}{\partial x_\beta} + \frac{\partial u_\beta}{\partial x_\alpha}\right)\rho & \\ = -2dS_{\alpha\beta} - 2P_{\alpha\beta 31} w_x + \partial_x \left(P_{\alpha\beta 13} - \frac{1}{d}\delta_{\alpha\beta} S_{13}\right). & \end{aligned} \tag{3.5}$$

Now we approximate $P_{\alpha\beta 31}$ according to (3.3) and obtain the nonlinear moment closure model equations

$$\begin{aligned} \partial_t \rho &= \partial_x S_{13} \\ \partial_t S_{11} - \left(\frac{3}{7} - \frac{1}{d}\right)\partial_x S_{13} &= -2dS_{11} - \frac{6}{7} w_x S_{13} \\ \partial_t S_{22} - \left(\frac{1}{7} - \frac{1}{d}\right)\partial_x S_{13} &= -2dS_{22} - \frac{2}{7} w_x S_{13} \\ \partial_t S_{33} - \left(\frac{3}{7} - \frac{1}{d}\right)\partial_x S_{13} &= -2dS_{33} + \frac{8}{7} w_x S_{13} \\ \partial_t S_{13} + \frac{1}{7}\partial_x S_{22} &= -2dS_{13} + w_x\left(S_{11} + \frac{2}{7}S_{22}\right) + w_x \rho\left(-\frac{2}{15} + \frac{1}{d}\right) + \frac{1}{15}\partial_x \rho, \end{aligned} \tag{3.6}$$

which need to be solved together with the Stokes or Navier-Stokes equations. The evolution equations for S_{12} and S_{23} are decoupled from the system (3.6) and can be neglected.

3.4. Rectilinear flow. Now we restrict our considerations to a rectilinear flow, i.e. taking the form

$$\begin{aligned} f &= f(t, x, y, \boldsymbol{n}) \\ \boldsymbol{u} &= (0, 0, w(t, x, y))^T \\ S &= S(t, x, y) \end{aligned} \tag{3.7}$$

Furthermore, we consider again the case $\gamma = 0$. Under these assumptions, the system (3.2) can be written in the form

$$\begin{aligned}
&\partial_t \rho = \partial_x S_{13} + \partial_y S_{23} \\
&\partial_t S_{\alpha\beta} - \frac{\partial u_\alpha}{\partial x} S_{1\beta} - \frac{\partial u_\alpha}{\partial y} S_{2\beta} - \frac{\partial u_\beta}{\partial x} S_{\alpha 1} - \frac{\partial u_\beta}{\partial y} S_{\alpha 2} - \frac{1}{d}\left(\frac{\partial u_\alpha}{\partial x_\beta} + \frac{\partial u_\beta}{\partial x_\alpha}\right)\rho \\
&= -2dS_{\alpha\beta} - 2w_x P_{\alpha\beta 31} - 2w_y P_{\alpha\beta 32} + \partial_x\left(P_{\alpha\beta 13} - \frac{1}{d}\delta_{\alpha\beta} S_{13}\right) + \partial_y\left(P_{\alpha\beta 23} - \frac{1}{d}\delta_{\alpha\beta} S_{23}\right)
\end{aligned} \tag{3.8}$$

Using the approximation (3.3), we obtain the nonlinear moment closure for rectilinear flow

$$\begin{aligned}
\partial_t \rho &= \partial_x S_{13} + \partial_y S_{23} \\
\partial_t S_{11} + 2dS_{11} &= (-2w_x + \partial_x)\frac{3}{7} S_{13} + (-2w_y + \partial_y)\frac{1}{7} S_{23} - \frac{1}{d}(\partial_x S_{13} + \partial_y S_{23}) \\
\partial_t S_{22} + 2dS_{22} &= (-2w_x + \partial_x)\frac{1}{7} S_{13} + (-2w_y + \partial_y)\frac{3}{7} S_{23} - \frac{1}{d}(\partial_x S_{13} + \partial_y S_{23}) \\
\partial_t S_{33} + 2dS_{33} &= 2w_x S_{13} + 2w_y S_{23} + (-2w_x + \partial_x)\frac{3}{7} S_{13} + (-2w_y + \partial_y)\frac{3}{7} S_{23} - \frac{1}{d}(\partial_x S_{13} + \partial_y S_{23}) \\
\partial_t S_{13} + 2dS_{13} &= (S_{11} + \frac{\rho}{d}) w_x + S_{12} w_y + (-2w_x + \partial_x)\left(-\frac{1}{7} S_{22} + \frac{\rho}{15}\right) + (-2w_y + \partial_y)\frac{1}{7} S_{12} \\
\partial_t S_{23} + 2dS_{23} &= w_x S_{12} + w_y\left(S_{22} + \frac{\rho}{d}\right) + (-2w_x + \partial_x)\frac{1}{7} S_{12} + (-2w_y + \partial_y)\left(-\frac{1}{7} S_{11} + \frac{\rho}{15}\right) \\
\partial_t S_{12} + 2dS_{12} &= (-2w_x + \partial_x)\frac{1}{7} S_{23} + (-2w_y + \partial_y)\frac{1}{7} S_{13},
\end{aligned} \tag{3.9}$$

which should be solved together with the macroscopic Stokes or Navier-Stokes equations.

4. Derivation of an effective equation via a quasi-dynamic approximation. In this section, we derive a scalar evolution equation for the particle density ρ, which describes the cluster formation process for intermediate and long times. We will separately consider shear flow and rectilinear flow. The computation is much simpler for the shear flow and it serves as a pedagogical example to explain the main approximation idea.

4.1. Shear flow. We consider the system (3.6) describing a shear flow. The rods are allowed to move out of the plane of the shear and $\boldsymbol{n}$ takes values on the sphere S^2, hence $d = 3$. The system then is written as

$$\partial_t \rho = \partial_x S_{13} \tag{4.1}$$

$$\partial_t S + A\partial_x S = LS + f(w_x, \rho, \rho_x), \tag{4.2}$$

where $S = (S_{11}, S_{22}, S_{33}, S_{13})^T$,

$$f(w_x, \rho, \rho_x) = \left(0, 0, 0, \left(\tfrac{3}{15} w_x \rho + \tfrac{1}{15}\rho_x\right)\right)^T$$

,

$$A = \begin{pmatrix} 0 & 0 & 0 & \frac{1}{3} - \frac{3}{7} \\ 0 & 0 & 0 & \frac{1}{3} - \frac{1}{7} \\ 0 & 0 & 0 & \frac{1}{3} - \frac{3}{7} \\ 0 & \frac{1}{7} & 0 & 0 \end{pmatrix}, \quad L = \begin{pmatrix} -6 & 0 & 0 & -\frac{6}{7} w_x \\ 0 & -6 & 0 & -\frac{2}{7} w_x \\ 0 & 0 & -6 & \frac{8}{7} w_x \\ w_x & \frac{2}{7} w_x & 0 & -6 \end{pmatrix}. \tag{4.3}$$

The idea of the quasi-dynamic approximation is the following: the density ρ is generated by the 0-th order harmonic polynomials associated to the eigenvalue $\lambda_0 = 0$ of the Laplace-Beltrami operator; the

stresses S_{ij} are generated by the 2-nd order spherical harmonics s_{ij} which are eigenfunctions of Laplace-Beltrami associated to the common eigenvalue $\lambda = -6$. The stresses are thus expected to decay faster; similarly higher-order harmonics that are neglected in (3.6) are expected to decay even faster. We split the system according to the decay rates of the modes in (4.1), (4.2) and set the faster decaying modes to their local equilibrium; we call this approximation quasi-dynamic approximation since part of the modes evolve dynamically while the rest of the modes are relaxed immediately to their local equilibrium values.

To accomplish that we set (4.2) to its equilibrium $LS + f(w_x, \rho, \rho_x) = 0$ and the dynamics of (3.6) is approximated by

$$\begin{aligned} \partial_t \rho &= \partial_x S_{13} \\ S_{11} + \frac{6}{42} w_x S_{13} &= 0 \\ S_{22} + \frac{2}{42} w_x S_{13} &= 0 \\ S_{33} - \frac{8}{42} w_x S_{13} &= 0 \\ -\frac{7}{42} w_x S_{11} - \frac{2}{42} w_x S_{22} + S_{13} &= \tfrac{1}{90}(3\rho w_x + \rho_x) \end{aligned} \tag{4.4}$$

As already mentioned, the underlying thinking is that $(S_{11}, S_{22}, S_{33}, S_{13})$ relax fast to their local equilibria, since their decay rate (at least near equilibrium) is determined by the first nonzero eigenvalue of the Laplace-Beltrami operator, while ρ does not relax, as it corresponds to the eigenvalue $\lambda_0 = 0$ of the Laplace Beltrami operator.

Solving the algebraic equation in (4.4), we obtain

$$S_{13} = \tfrac{\kappa}{90} \frac{1}{\kappa + 46 w_x^2} \big(3\rho w_x + \rho_x\big) \qquad \text{where } \kappa = 42^2 \,. \tag{4.5}$$

The effective equation for the evolution of ρ then has the form

$$\partial_t \rho = \partial_x \left(\tfrac{\kappa}{90} \frac{1}{\kappa + 46 w_x^2} \big(3\rho w_x + \rho_x\big) \right) \tag{4.6}$$

which needs to be solved together with the Stokes or Navier-Stokes equation for shear flow

$$Re\, \partial_t w(t,x) = \partial_{xx} w(t,x) + \delta\,(m - \rho)\,. \tag{4.7}$$

The system (4.6)-(4.7) should be compared to the Keller-Segel model (*e.g.* [18, 12, 1]) that has been extensively used as a model for chemotaxis in biology. Compared to the Keller-Segel model, the present system has the noteworthy difference that the convection and diffusion coefficients in (4.6) depend nonlinearly on the gradient of the "potential" (played here by the shear w_x) and are in fact decreasing for increasing shear. It is an example within the general class of flux-limited systems proposed in [6], [30, 24] as models for flux-limited diffusion, although strictly speaking the present model is not included in the models listed in the above references and has the feature to be endowed with both flux-limited convection and diffusion. An extension that also presents anisotropic diffusion is developed in the next section to describe cluster formation for rectilinear flows.

4.2. Rectilinear flow. For rectilinear flows we again apply the quasidynamic approximation, similar in spirit as for shear flows but now requiring more cumbersome calculations. We rewrite equation (3.9) in the form

$$\begin{aligned} \partial_t \rho &= \partial_x S_{13} + \partial_y S_{23} \\ \partial_t S + A_x \partial_x S + B_y \partial_y S &= LS + f(w_x, w_y, \rho, \rho_x, \rho_y), \end{aligned} \tag{4.8}$$

with $S = (S_{11}, S_{22}, S_{33}, S_{13}, S_{23}, S_{12})^T$, $d = 3$ and $\boldsymbol{n}$ taking values in S^2,

$$A_x = \begin{pmatrix} 0 & 0 & 0 & \frac{1}{3}-\frac{3}{7} & 0 & 0 \\ 0 & 0 & 0 & \frac{1}{3}-\frac{1}{7} & 0 & 0 \\ 0 & 0 & 0 & \frac{1}{3}-\frac{3}{7} & 0 & 0 \\ 0 & \frac{1}{7} & 0 & 0 & 0 & 0 \\ 0 & 0 & 0 & 0 & 0 & -\frac{1}{7} \\ 0 & 0 & 0 & 0 & -\frac{1}{7} & 0 \end{pmatrix}, \quad B_y = \begin{pmatrix} 0 & 0 & 0 & 0 & \frac{1}{3}-\frac{1}{7} & 0 \\ 0 & 0 & 0 & 0 & \frac{1}{3}-\frac{3}{7} & 0 \\ 0 & 0 & 0 & 0 & \frac{1}{3}-\frac{3}{7} & 0 \\ 0 & 0 & 0 & 0 & 0 & -\frac{1}{7} \\ \frac{1}{7} & 0 & 0 & 0 & 0 & 0 \\ 0 & 0 & 0 & -\frac{1}{7} & 0 & 0 \end{pmatrix}, \tag{4.9}$$

$$L = \begin{pmatrix} -6 & 0 & 0 & -\frac{6}{7}w_x & -\frac{2}{7}w_y & 0 \\ 0 & -6 & 0 & -\frac{2}{7}w_x & -\frac{6}{7}w_y & 0 \\ 0 & 0 & -6 & \frac{8}{7}w_x & \frac{8}{7}w_y & 0 \\ w_x & \frac{2}{7}w_x & 0 & -6 & 0 & \frac{5}{7}w_y \\ \frac{2}{7}w_y & w_y & 0 & 0 & -6 & \frac{5}{7}w_x \\ 0 & 0 & 0 & -\frac{2}{7}w_y & -\frac{2}{7}w_x & -6 \end{pmatrix}, \quad f = \begin{pmatrix} 0 \\ 0 \\ 0 \\ \frac{3}{15}w_x\rho + \frac{1}{15}\rho_x \\ \frac{3}{15}w_y\rho + \frac{1}{15}\rho_y \\ 0 \end{pmatrix}. \tag{4.10}$$

The quasi–dynamic approximation is obtained by setting the second equation of (4.8) to its local equilibrium, i.e. the solution of

$$LS + f(\nabla w, \rho, \nabla\rho) = 0\,. \tag{4.11}$$

After some manipulations this leads to solving for (S_{13}, S_{23}) the algebraic system

$$\begin{aligned} (\kappa + 10(w_x^2 + w_y^2) + 36w_x^2)S_{13} + 36w_xw_yS_{23} &= \tfrac{\kappa}{30}(w_x\rho + \tfrac{1}{3}\rho_x) \\ 36w_xw_yS_{13} + (\kappa + 10(w_x^2 + w_y^2) + 36w_y^2)S_{23} &= \tfrac{\kappa}{30}(w_y\rho + \tfrac{1}{3}\rho_y)\,, \end{aligned} \tag{4.12}$$

where $\kappa = 42^2$, and evaluating the remaining stresses via

$$\begin{aligned} S_{11} &= -\tfrac{6}{42}w_xS_{13} - \tfrac{2}{42}w_yS_{23} \\ S_{22} &= -\tfrac{2}{42}w_xS_{13} - \tfrac{6}{42}w_yS_{23} \\ S_{23} &= \tfrac{8}{42}w_xS_{13} + \tfrac{8}{42}w_yS_{23} \\ S_{12} &= -\tfrac{2}{42}w_yS_{13} - \tfrac{2}{42}w_xS_{23}\,. \end{aligned} \tag{4.13}$$

The solution of the algebraic system (4.12) is expressed in the form

$$\begin{pmatrix} S_{13} \\ S_{23} \end{pmatrix} = D(\nabla w)\,\tfrac{\kappa}{30}\rho\nabla\Big(w + \tfrac{1}{3}\ln\rho\Big)\,, \tag{4.14}$$

where $\nabla = (\partial_x, \partial_y)$, and $D(\nabla w)$ is a matrix obtained by inverting (4.12) and given in the successive forms

$$\begin{aligned} D(\nabla w) &:= \frac{1}{(\kappa + 10|\nabla w|^2)(\kappa + 46|\nabla w|^2)} \begin{pmatrix} \kappa + 10|\nabla w|^2 + 36w_y^2 & -36w_xw_y \\ -36w_xw_y & \kappa + 10|\nabla w|^2 + 36w_x^2 \end{pmatrix} \\ &= \frac{1}{\kappa + 10|\nabla w|^2}\left[I - \frac{36}{\kappa + 46|\nabla w|^2}\,\nabla w \otimes \nabla w\right] \\ &= \frac{1}{\kappa + 46|\nabla w|^2}\Big[I + \frac{36}{\kappa + 10|\nabla w|^2}\big(|\nabla w|^2 I - \nabla w \otimes \nabla w\big)\Big] \end{aligned} \tag{4.15}$$

When (4.14) is introduced into $(4.8)_1$ we obtain the non-isotropic diffusion equation

$$\partial_t\rho = \nabla \cdot \big(D(\nabla w)\tfrac{\kappa}{30}\rho\nabla\big(w + \tfrac{1}{3}\ln\rho\big)\big)\,, \tag{4.16}$$

which is conjectured to describe the effective response of the system.

4.3. The effective equation for rectilinear flow. Combining $(4.8)_1$ with (4.14), (4.15) and (2.37) (for $\gamma = 0$), we obtain the effective equation describing the dynamics of the rectilinear sedimenting flow. This takes the form

$$\begin{aligned} \partial_t \rho &= \nabla \cdot \left(\frac{1}{\kappa + 10|\nabla w|^2} \Big[I - \frac{36}{\kappa + 46|\nabla w|^2} \, \nabla w \otimes \nabla w \Big] \tfrac{\kappa}{30} \rho \nabla \big(w + \tfrac{1}{3} \ln \rho \big) \right) \\ Re \, \partial_t w &= \triangle_{(x,y)} w + \delta \, (\bar\rho - \rho) \end{aligned} \tag{4.17}$$

The constant $\bar\rho$ is selected to be either the initial mass over a period (if the problem is periodic) or the total mass $\bar\rho = \int \rho(x,t) dx$ (for the Cauchy problem). In either case the mass is conserved and the selection of $\bar\rho$ amounts to a change of Galilean frame for observing the flow.

Equation $(4.17)_1$ describes anisotropic diffusion. The diffusion matrix $D(\nabla w)$ in (4.15) is symmetric and positive definite. The system (4.17) is invariant under rotations in the x, y-plane. Indeed, for $x' = Qx$ with $Q \in SO(2)$, we have $\nabla_{x'} = Q^T \nabla_x$ and $|\nabla_x w| = |Q \nabla_{x'} w| = |\nabla_{x'} w|$. Then (4.15) implies

$$D(\nabla_x w) = D(Q \nabla_{x'} w) = Q D(\nabla_{x'} w) Q^T$$

and $(4.17)_1$ is invariant,

$$\begin{aligned} \partial_t \rho &= Q \nabla_{x'} \cdot Q D(\nabla_{x'} w) Q^T \tfrac{\kappa}{30} \rho Q \nabla_{x'} \big(w + \tfrac{1}{3} \ln \rho \big) \\ &= \nabla_{x'} \cdot D(\nabla_{x'} w) \tfrac{\kappa}{30} \rho \nabla_{x'} \big(w + \tfrac{1}{3} \ln \rho \big) \end{aligned}$$

The same is true for $(4.17)_2$ due to the invariance of the Laplacian under rotations.

Finally, we show that (4.17) is endowed with an entropy-dissipation structure. For concreteness, we assume periodic boundary conditions over a domain of periodicity $\mathbb{T}$. The total density is then conserved, and we select $\bar\rho$ in $(4.17)_2$ as

$$\bar\rho = \int_{\mathbb{T}} \rho(x,t) dx = \int_{\mathbb{T}} \rho_0(x) dx \, .$$

Note that this choice can be always assured by changing Galilean frame of reference. Moreover,

$$\int_{\mathbb{T}} w_t dx = 0 \, , \quad \int_{\mathbb{T}} w(x,t) dx = \int_T w_0(x) dx$$

Next, we multiply $(4.17)_1$ by $\frac{1}{3}(1 + \ln \rho) + w$ and $(4.17)_2$ by w_t ; after some integrations by part we respectively obtain

$$\begin{aligned} \partial_t \big(\tfrac{1}{3} \rho \ln \rho + \rho w \big) - \rho w_t &= \nabla \cdot \big(\tfrac{1}{3}(1 + \ln \rho) + w \big) \tfrac{\kappa}{30} \rho D(\nabla w) \nabla \big(w + \tfrac{1}{3} \ln \rho \big) \\ &\quad - \nabla \big(w + \tfrac{1}{3} \ln \rho \big) \cdot \tfrac{\kappa}{30} \rho D(\nabla w) \, \nabla \big(w + \tfrac{1}{3} \ln \rho \big) \\ \rho w_t + Re \, w_t^2 + \partial_t \tfrac{1}{2} |\nabla w|^2 &= \nabla \cdot w_t \nabla w + \delta \bar\rho w_t \end{aligned}$$

and the entropy (free-energy) dissipation identity

$$\begin{aligned} &\frac{d}{dt} \int_{\mathbb{T}} \big(\tfrac{1}{3} \rho \ln \rho + \rho w + \tfrac{1}{2} |\nabla w|^2 \big) dx \\ &\qquad + \int_{\mathbb{T}} \big[Re \, w_t^2 + \nabla \big(w + \tfrac{1}{3} \ln \rho \big) \cdot \tfrac{\kappa}{30} \rho D(\nabla w) \, \nabla \big(w + \tfrac{1}{3} \ln \rho \big) \big] \, dx = 0 \, . \end{aligned} \tag{4.18}$$

4.4. Remarks concerning the validity of the quasidynamic approximation. The validity of the conjecture that the long time dynamics of (4.8) together with Stokes is described by the system (4.17) is at present an open problem. In the sequel, we take up the case of rectilinear flows, and give some partial arguments highlighting the idea and the analytical difficulties for justifying the quasidynamic approximation. Then, in the following section, we will restrict to the case of shear flows, and give numerical evidence that shows that the quasidynamic approximation is a good representation of the full dynamics of the kinetic model for long times, and will present a heuristic argument towards justifying the approximation for shear flows.

The idea behind the approximation is that the transient dynamics of S is replaced by its equilibrium response. This amounts to considering the simplified linear non-homogeneous problem

$$\partial_t S + A_x \partial_x S + B_y \partial_y S = LS + f(x)$$

and postulating that its solution is well approximated for long-times by its local equilibrium

$$LS + f(x) = 0\,.$$

This would be the case provided the solutions of the homogeneous system

$$\partial_t S + A_x \partial_x S + B_y \partial_y S - LS = 0 \tag{4.19}$$

decay to zero for large times, *i.e.* $S(x,t) \to 0$ as $t \to \infty$.

The solution of (4.19) can be visualised as the Trotter product of the semigroup generated by the system of ordinary differential equations

$$\partial_t S - LS = 0 \tag{4.20}$$

and the semigroup generated by the linear hyperbolic system

$$\partial_t S + A_x \partial_x S + B_y \partial_y S = 0\,. \tag{4.21}$$

The eigenvalues of (4.20) are computed by finding the roots of the characteristic polynomial $\det(-\lambda I + L) = 0$ where

$$L - \lambda I = \begin{pmatrix} -(\lambda+6) & 0 & 0 & -\frac{6}{7}w_x & -\frac{2}{7}w_y & 0 \\ 0 & -(\lambda+6) & 0 & -\frac{2}{7}w_x & -\frac{6}{7}w_y & 0 \\ 0 & 0 & -(\lambda+6) & \frac{8}{7}w_x & \frac{8}{7}w_y & 0 \\ w_x & \frac{2}{7}w_x & 0 & -(\lambda+6) & 0 & \frac{5}{7}w_y \\ \frac{2}{7}w_y & w_y & 0 & 0 & -(\lambda+6) & \frac{5}{7}w_x \\ 0 & 0 & 0 & -\frac{2}{7}w_y & -\frac{2}{7}w_x & -(\lambda+6) \end{pmatrix}. \tag{4.22}$$

They can be computed via the following formula: If A, B, C, D are square matrices of the same size and the matrix A is invertible, then

$$K := \begin{pmatrix} A & B \\ C & D \end{pmatrix} = \begin{pmatrix} A & 0 \\ C & I \end{pmatrix} \begin{pmatrix} I & A^{-1}B \\ 0 & D - CA^{-1}B \end{pmatrix}$$

and

$$\det K = \det A \det(D - CA^{-1}B) \tag{4.23}$$

Using this formula, a lengthy but straightforward calculation yields that the six eigenvalues of (4.20) are

$$\begin{cases} \lambda_{1,2} = -6 \quad \text{with multiplicity 2} \\ \lambda_{3,4} = -6 \pm \imath \frac{\sqrt{46}}{7} \sqrt{w_x^2 + w_y^2} \\ \lambda_{5,6} = -6 \pm \imath \frac{\sqrt{10}}{7} \sqrt{w_x^2 + w_y^2} \end{cases}$$

All the eigenvalues have strictly negative real parts and the solution of (4.20) converges to zero as $t \to \infty$.

The same formula can be used to calculate the eigenvalues of (4.21) and establish that this system is hyperbolic. Indeed, for a vector $\nu = (\nu_x, \nu_y) \in \mathbb{R}^2$, $\nu \neq 0$, we use formula (4.23) and compute that the eigenvalues of $(-\lambda I + \nu_x A_x + \nu_y B_y)$ are

$$\begin{cases} \lambda_{1,2} = 0 \quad \text{ of multiplicity } 2 \\ \lambda_{3,4} = \pm \frac{2}{7\sqrt{3}} \sqrt{\nu_x^2 + \nu_y^2} \\ \lambda_{5,6} = \pm \frac{1}{7} \sqrt{\nu_x^2 + \nu_y^2} \end{cases}$$

One easily checks that the eigenspace corresponding to the zero-eigenvalue is two-dimensional. The problem (4.21) is hence hyperbolic. It is tempting to conclude that S converges to zero as time tends to infinity. Such results are available when the matrices A_x and B_y are symmetric (see [27]), but we are not aware of a corresponding theory covering the case that the matrices A_x and B_y are not symmetric. We have not been able to compute the eigenvalues for the full homogeneous problem (4.19), what would provide a quantitative criterion for what flows the quasidynamic approximation is valid. Our conjecture is that the validity of the approximation extends to flows where $|\nabla w|$ remains moderate. This conjecture is justified in the following section for shear flows and is consistent with the numerical simulations of section 4.6.

4.5. Justification for shear flows. To justify the quasidynamic approximation for shear flow, we show that for moderate values of $|w_x|$ solutions of the homogeneous system

$$\partial_t S + A \partial_x S - LS = 0, \tag{4.24}$$

with A and L as described in (4.3) decay to zero for large times. We look for solutions of the form

$$S(x,t) = r \exp(\lambda t + ikx), \tag{4.25}$$

with $\lambda, k \in \mathbb{R} \setminus \{0\}$. Computing such solutions amounts to finding eigenvalues λ and eigenvectors r for the problem

$$(\lambda I + ikA - L)r = 0.$$

The solutions $S(x,t)$ of (4.24) decay to zero, if $\mathrm{Re}(\lambda) < 0$ for all possible solutions λ, r of (4.25). We find that λ has the form

$$\begin{aligned} &\lambda_{1,2} = -6 \pm \frac{1}{21}\kappa, \quad \text{with } \kappa := \sqrt{36ikw_x - 12k^2 - 414w_x^2} \\ &\lambda_{3,4} = -6. \end{aligned} \tag{4.26}$$

Corresponding eigenvectors are given by

$$r_1 = \frac{1}{\kappa} \begin{pmatrix} 2(ik - 9w_x) \\ -2(2ik + 3w_x) \\ 2(ik + 12w_x) \\ \kappa \end{pmatrix}, \; r_2 = \frac{1}{\kappa} \begin{pmatrix} -2(ik - 9w_x) \\ 2(2ik + 3w_x) \\ -2(ik + 12w_x) \\ \kappa \end{pmatrix}, r_3 = \begin{pmatrix} 0 \\ 0 \\ 1 \\ 0 \end{pmatrix}, r_4 = \begin{pmatrix} \frac{ik - 2w_x}{7w_x} \\ 1 \\ 0 \\ 0 \end{pmatrix} \tag{4.27}$$

Now we use the relation

$$Re(\sqrt{a + ib}) = \sqrt{\frac{a + \sqrt{a^2 + b^2}}{2}}$$

in order to compute the real part of κ.

$$\begin{aligned}\mathrm{Re}(\kappa) &= \mathrm{Re}\left(\sqrt{-12k^2 - 414w_x^2 + 36ikw_x}\right)\\ &= \sqrt{\frac{-12k^2 - 414w_x^2 + \sqrt{12^2k^4 + 11232k^2w_x^2 + 414^2w_x^4}}{2}}\\ &< \sqrt{\frac{-12k^2 - 414w_x^2 + \sqrt{(12k^2 + 468w_x^2)^2}}{2}}\\ &= \sqrt{27}|w_x|\end{aligned}$$

Thus, $\mathrm{Re}(\lambda) < -6 + \frac{\sqrt{27}}{21}|w_x| < 0$ whenever $|w_x| < 14\sqrt{3}$.

Finally, we present numerical results for the shear flow problem, which confirm that the quasi-dynamic approximation leads to an accurate representation of the solution structure. We use the parameter values $D_r = \delta = Re = 1$ and $\gamma = 0$.

For shear flow, the full model has the form

$$\begin{aligned}&\partial_t f + \nabla_{\boldsymbol{n}} \cdot \left(P_{\boldsymbol{n}^\perp}(0,0,n_1w_x)^T f\right) - \partial_x\left(n_1n_2 f\right) = \Delta_{\boldsymbol{n}} f\\ &\partial_t w = \frac{\partial^2 w}{\partial x^2} + \left(m - \int_{S^2} f d\boldsymbol{n}\right).\end{aligned} \tag{4.28}$$

The effective equation for the evolution of ρ has the form

$$\begin{aligned}&\partial_t \rho = \partial_x\left(\frac{\kappa}{90}\frac{1}{\kappa + 46w_x^2}(3\rho w_x + \rho_x)\right) \quad (\kappa = 42^2)\\ &w_t = w_{xx} + (m - \rho).\end{aligned} \tag{4.29}$$

Furthermore, we compare the simulations of the full model (4.28) with results for the nonlinear moment closure (3.6) and the linear model

$$\begin{aligned}\partial_t\rho - \partial_x S_{13} &= 0\\ \partial_t S_{11} - \frac{2}{21}\partial_x S_{13} &= -6S_{11}\\ \partial_t S_{22} + \frac{4}{7}\partial_x S_{13} &= -6S_{22}\\ \partial_t S_{33} - \frac{2}{21}\partial_x S_{13} &= -6S_{33}\\ \partial_t S_{13} + \frac{1}{7}\partial_x S_{22} - \frac{1}{15}\partial_x\rho &= -6S_{13} + \frac{1}{5}\partial_x w\\ \partial_t w &= \partial_{xx} w + (m - \rho),\end{aligned} \tag{4.30}$$

which is obtained by linearizing the nonlinear moment closure model around the state $\rho = 1$ and $w = 0$.

We compute periodic solutions on the intervall $0 \le x \le 100$. The computational domain in the x-direction is discretized with 400 grid cells. The initial values are set to be

$$\rho(x_k, 0) = 1 + 10^{-4}\left(\epsilon(x_k) - \frac{1}{2}\right),$$

where $\epsilon(x_k)$ is a random number between 0 and 1 and $k = 1, \ldots, 400$. The initial values for the velocity are set to zero, i.e. $w(x, 0) = 0$. Figure 4.1 shows plots of the initial values.

In our simulations of the full model, the initial values for f are set to be

$$f(x_k, 0, \boldsymbol{n}) = \frac{\rho(x_k)}{4\pi}, \quad k = 1, \ldots, 400, \boldsymbol{n} \in S^2$$

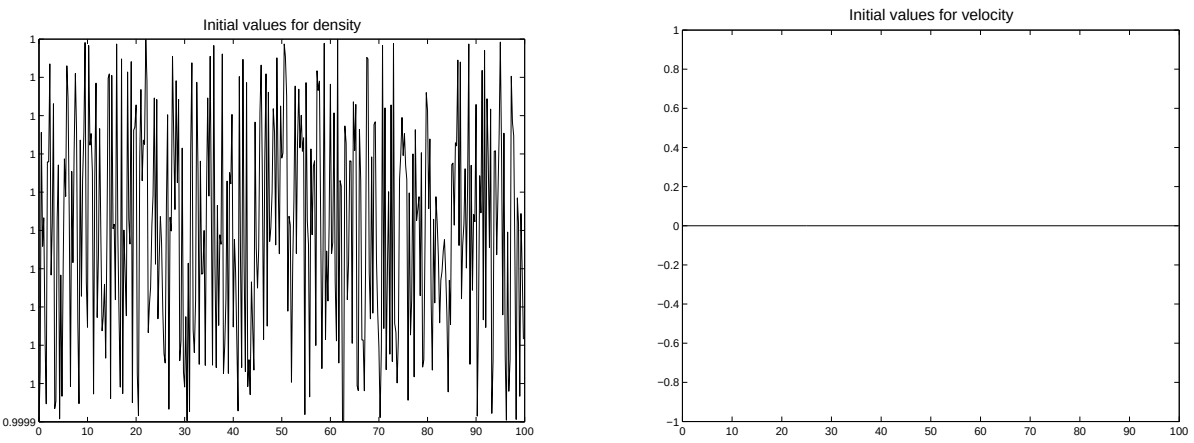

FIG. 4.1. *Initial values for ρ and w.*

In the simulations of the nonlinear and the linear moment closure model, the initial values for $S_{11}, S_{22}, S_{33}, S_{13}$ are computed via the relation

$$S_{ij}(x_k, 0) = \int_{S^2} \left(n_i n_j - \frac{1}{3}\delta_{ij} \right) f(x_k, 0, \boldsymbol{n}) d\boldsymbol{n}, \quad k = 1, \ldots, 400.$$

Figures 4.2-4.4 present the results of our numerical simulations. In all of these plots, the black line is the density ρ or the absolute value of velocity gradient $|w_x|$ as computed from the full model. This solution is compared with results of the nonlinear moment closure model (red dashed curves in the left plots), the linear moment closure model (red dashed curve in the middle plots) as well as with results of the quasidynamic approximation (red dashed curve in the right plots).

For small times, i.e. the linear regime shown in Figure 4.2, we see that all models provide an accurate prediction of the solution structure. At later times as shown in Figure 4.3, nonlinear effects start to become important and the linear moment closure model becomes less accurate. At even later times, as shown in Figure 4.4, the predictions of the linear model are inaccurate, while the nonlinear moment closure as well as the quasidynamic approximation lead to an accurate prediction of the solution structure. Note however, that the linear model provides a good prediction of the number of clusters which appear.

4.6. Numerical simulations for rectilinear flow. We also show numerical simulations for rectilinear flow, comparing the nonlinear moment closure system (3.9) with the quasidynamic approximation (4.17). So far we don't have numerical results for the full model in the rectilinear flow case. Note that the full model is a four-dimensional time-dependent problem, requiring the solution of a drift-diffusion equation on the sphere in each grid cell of a two-dimensional mesh and during each time step.

Our numerical results for rectilinear flow agree well with the findings for shear flow. Starting with a quiescent flow and a uniform distribution of rod orientations with a randomly perturbed density around $\rho = 1$, we observe the formation of clusters with higher particle density. Furthermore, we observe that the nonlinear moment closure model and the quasidynamic approximation leads to very similar results.

For our numerical results shown in Figure 4.5 we used the parameter values $Re = \delta = 1$ and show density and velocity gradient $\sqrt{w_x^2 + w_y^2}$ at time $t = 450$.

Appendices. Appendix A. Harmonic Polynomials and Spherical Harmonics.

For the reader's convenience we review some material on harmonic polynomials and spherical harmonics that is used in the text. We refer to Stein and Weiss [28, Ch 4] and Helgason [10, Intro Thm 3.1] for further details.

Let $\mathcal{P}_k(\mathbb{R}^d)$ be the space of homogeneous polynomials of degree k on $\mathbb{R}^d$. We denote by $\mathcal{P}_k(S^{d-1})$ the restrictions of polynomials $P \in \mathcal{P}_k(\mathbb{R}^d)$ on the sphere S^{d-1}. The dimension $dim\mathcal{P}_k(\mathbb{R}^d) = \binom{d+k-1}{k}$.

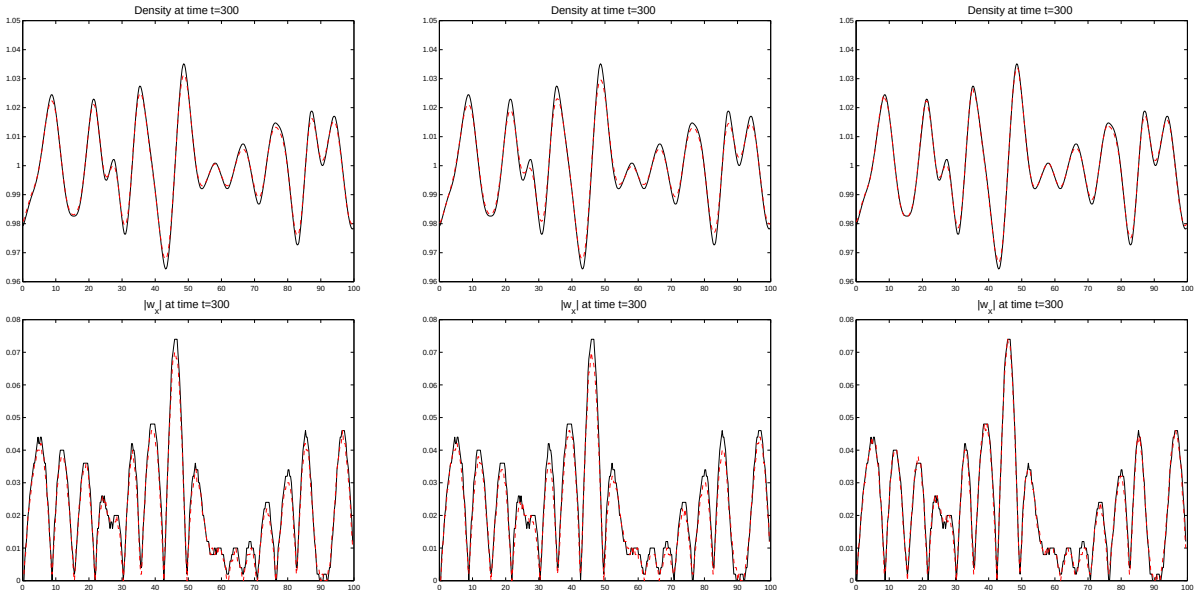

FIG. 4.2. *Numerical results comparing the full model (black solid line) with (left) the nonlinear moment closure, (middle) the linear moment closure, and (right) the quasidynamic approximation. The results of the macroscopic models are shown as red dashed line. Top line shows results for density, bottom line shows results for the absolut value of the velocity gradient.*

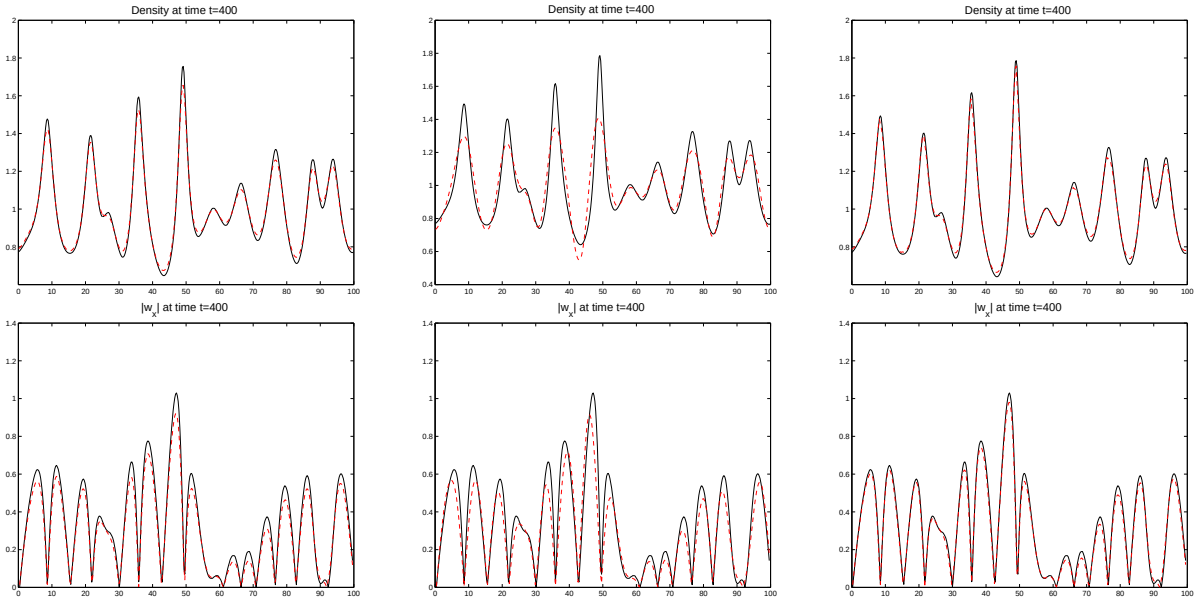

FIG. 4.3. *Numerical results comparing the full model (black solid line) with (left) the nonlinear moment closure, (middle) the linear moment closure, and (right) the quasidynamic approximation.*

Let $\mathcal{H}_k(\mathbb{R}^d)$ be the space of homogeneous polynomials of degree k on $\mathbb{R}^d$ that are harmonic,

$$\mathcal{H}_k(\mathbb{R}^d) = \{P \in \mathcal{P}_k(\mathbb{R}^d) : \triangle P = 0\}.$$

The elements of $\mathcal{H}_k(\mathbb{R}^d)$ are called solid harmonics. The spherical harmonics $\mathcal{H}_k(S^{d-1})$ are defined as the restrictions of $P \in \mathcal{H}_k(\mathbb{R}^d)$ on the sphere. The map $\rho : \mathcal{H}_k(\mathbb{R}^d) \to \mathcal{H}_k(S^{d-1})$ that maps the above polynomial to its restriction is a bijection.

The relation between these spaces of polynomials is given by the following proposition.

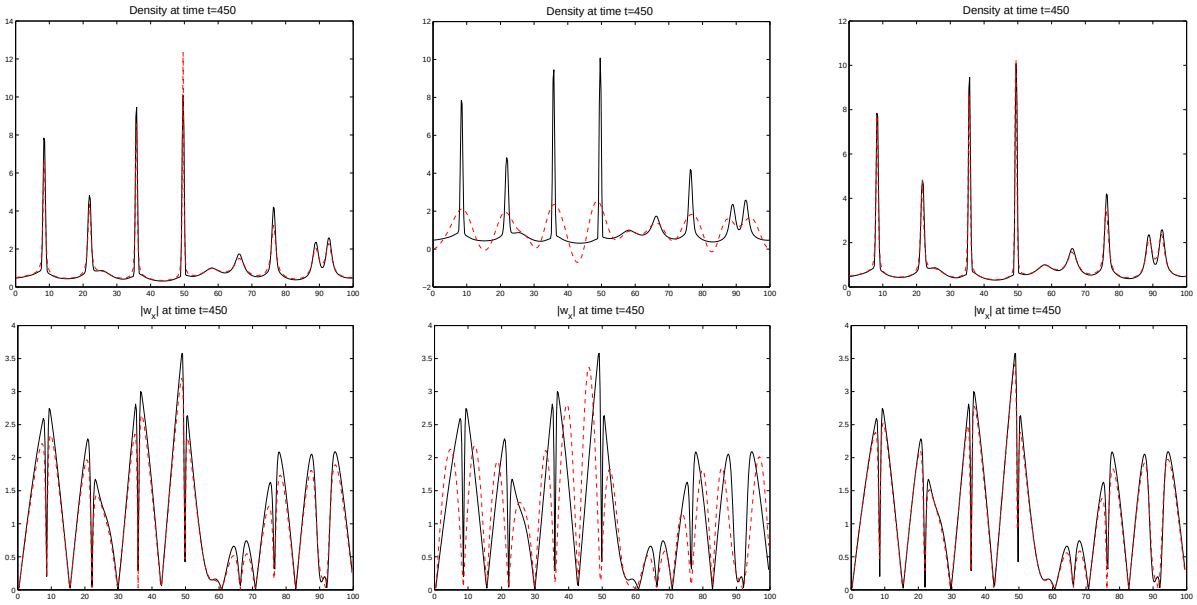

FIG. 4.4. *Numerical results comparing the full model (black solid line) with (left) the nonlinear moment closure, (middle) the linear moment closure, and (right) the quasidynamic approximation.*

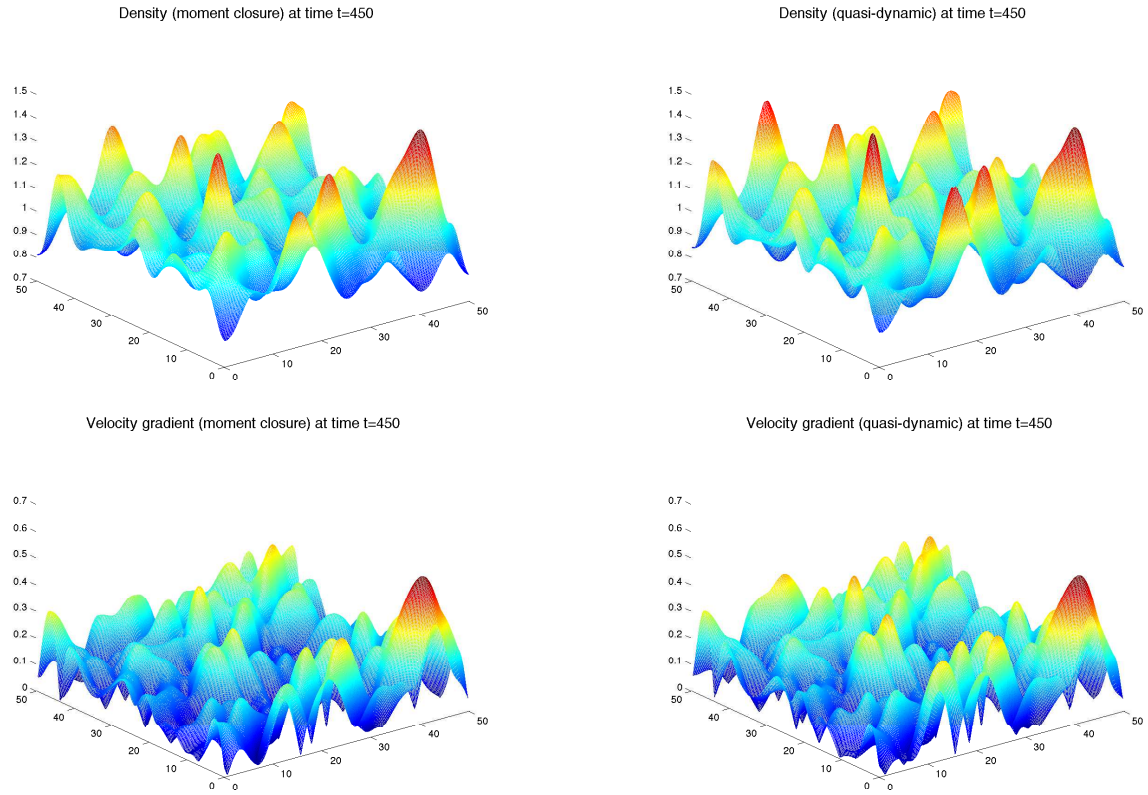

FIG. 4.5. *Numerical results for rectilinear flow, showing the density and the velocity gradient.*

THEOREM A.1. *The map* $\triangle : \mathcal{P}_k(\mathbb{R}^d) \to \mathcal{P}_{k-2}(\mathbb{R}^d)$ *is onto for all* d *and* $k \geq 2$. *Furthermore, we*

have the orthogonal direct sum decomposition

$$\mathcal{P}_k(\mathbb{R}^d) = \mathcal{H}_k(\mathbb{R}^d) \oplus |x|^2 \mathcal{P}_k(\mathbb{R}^d) \quad \textit{for } k \geq 2.$$

This proposition allows to compute the dimension of $\mathcal{H}_k(S^{d-1})$ as

$$\dim \mathcal{H}_k(\mathbb{R}^d) = \mathcal{H}_k(S^{d-1}) = \binom{d+k-1}{k} - \binom{d+k-3}{k-2} \quad \text{for } k \geq 2.$$

Note also that $\dim \mathcal{H}_0(\mathbb{R}^d) = 1$ and $\dim \mathcal{H}_1(\mathbb{R}^d) = d$. Moreover, proceeding via induction we deduce the direct sum decompositions

$$\mathcal{P}_k(\mathbb{R}^d) = \mathcal{H}_k(\mathbb{R}^d) \oplus |x|^2 \mathcal{H}_{k-2}(\mathbb{R}^d) \oplus ... \oplus |x|^{2\left[\frac{k}{2}\right]} \mathcal{H}_{k-2\left[\frac{k}{2}\right]}(\mathbb{R}^d) \tag{A.1}$$

$$\mathcal{P}_k(S^{d-1}) = \mathcal{H}_k(S^{d-1}) \oplus \mathcal{H}_{k-2}(S^{d-1}) \oplus ... \oplus \mathcal{H}_{k-2\left[\frac{k}{2}\right]}(S^{d-1}) \tag{A.2}$$

The importance of spherical harmonics stems from the property that for $P \in \mathcal{H}_k(\mathbb{R}^d)$ the restriction $H = P\Big|_{S^{d-1}} \in \mathcal{H}_k(S^{d-1})$ is an eigenfunction of the Laplace-Beltrami operator $\triangle_{S^{d-1}}$. To see that for $P \in \mathcal{H}_k(\mathbb{R}^d)$ we write $x = rn$, with $r = |x|$ and $n = \frac{x}{|x|}$, and write $P(x) = P(rn) = r^d H(n)$. Recall that for $f \in C^\infty(\mathbb{R}^d)$ the Laplacian is expressed as

$$\triangle f = \frac{1}{r^{d-1}} \frac{\partial}{\partial r} \left(r^{d-1} \frac{\partial f}{\partial r} \right) + \frac{1}{r^2} \triangle_{S^{d-1}} f$$

Using this formula we compute

$$\triangle P = 0 \quad \Longleftrightarrow \quad \triangle_{S^{d-1}} H = -k(d+k-2)H$$

Moreover, one has the following theorem (see [10, Intro Thm 3.1]:

THEOREM A.2. *The eigenspaces of the Laplace-Beltrami operator $\triangle_{S^{d-1}}$ are the spaces of spherical harmonics $\mathcal{H}_k(S^{d-1})$ with associated eigenvalue -k (d+k-2). The eigenspaces are ortogonal and $L^2(S^{d-1})$ admits the direct sum decomposition*

$$L^2(S^{d-1}) = \bigoplus_{k=0}^{\infty} \mathcal{H}_k(S^{d-1}) \tag{A.3}$$

In the present context we are interested in functions on the sphere S^{d-1} that are even, that is $f(-n) = f(n)$. In this case the basis will only involve the even spherical harmonics and the direct sum in (A.3) will extend over the even integers. On S^2 the spherical harmonics are computed by using the Legendre and associated Legendre polynomials. In Table A we list the harmonic polynomial basis functions (up to order 4) that are used in the calculations of the present article.

Appendix B. Linear stability analysis. Experimental studies for the sedimentation of suspensions with rod-like particles [13, 14, 21] reveal the formation of packets of particles which seem to have a mesoscopic equilibrium width. Our goal is to give an explanation of this wave length selection mechanism based on linear stability theory.

We consider the linear pde for shear flow

$$\begin{aligned}
\partial_t \rho &= \partial_x S_{13} \\
\partial_t S_{11} &= \frac{2}{21} \partial_x S_{13} - 6 D_r S_{11} \\
\partial_t S_{22} &= -\frac{4}{7} \partial_x S_{13} - 6 D_r S_{22} \\
\partial_t S_{33} &= \frac{2}{21} \partial_x S_{13} - 6 D_r S_{33} \\
\partial_t S_{13} &= -\frac{1}{7} \partial_x S_{22} + \frac{1}{15} \partial_x \rho - 6 D_r S_{13} + \frac{1}{5} \partial_x w \\
Re\, \partial_t w &= \partial_{xx} w + \delta(m - \rho),
\end{aligned} \tag{B.1}$$

$0th$ order	$2nd$ order	$4th$ order
		$P_4^{-4} = \sin^4\theta\cos 4\phi$
		$P_4^{-3} = \sin^3\theta\cos\theta\cos 3\phi$
	$P_2^{-2} = \sin^2\theta\cos 2\phi$	$P_4^{-2} = \sin^2\theta(7\cos^2\theta - 1)\cos 2\phi$
	$P_2^{-1} = \sin\theta\cos\theta\cos\phi$	$P_4^{-1} = \sin\theta(7\cos^3\theta - 3\cos\theta)\cos\phi$
$P_0^0 = 1$	$P_2^0 = \cos^2\theta - \frac{1}{3}$	$P_4^0 = 35\cos^4\theta - 30\cos^2\theta + 3$
	$P_2^1 = \sin\theta\cos\theta\sin\phi$	$P_4^1 = \sin\theta(7\cos^3\theta - 3\cos\theta)\sin\phi$
	$P_2^2 = \sin^2\theta\sin 2\phi$	$P_4^2 = \sin^2\theta(7\cos^2\theta - 1)\sin 2\phi$
		$P_4^3 = \sin^3\theta\cos\theta\sin 3\phi$
		$P_4^4 = \sin^4\theta\sin 4\phi$

TABLE A.1
Harmonic polynomial basis functions.

which is obtained by linearizing the nonlinear moment closure system (3.6) around the state $\rho = 1$ and $\boldsymbol{u} = 0$.

Fourier transformation of the first five equations of (B.1) leads to the linear system of ordinary differential equations

$$\begin{aligned}
\hat{\rho}'(\xi,t) &= i\xi\hat{S}_{13}(\xi,t)\\
\hat{S}'_{11}(\xi,t) &= \frac{2}{21}i\xi\hat{S}_{13}(\xi,t) - 6D_r\hat{S}_{11}(\xi,t)\\
\hat{S}'_{22}(\xi,t) &= -\frac{4}{7}i\xi\hat{S}_{13}(\xi,t) - 6D_r\hat{S}_{22}(\xi,t)\\
\hat{S}'_{33}(\xi,t) &= \frac{2}{21}i\xi\hat{S}_{13}(\xi,t) - 6D_r\hat{S}_{33}(\xi,t)\\
\hat{S}'_{13}(\xi,t) &= -\frac{1}{7}i\xi\hat{S}_{22}(\xi,t) + \frac{1}{15}i\xi\hat{\rho}(\xi,t) - 6D_r\hat{S}_{13}(\xi,t) + \frac{1}{5}i\xi\hat{w}(\xi,t).
\end{aligned} \tag{B.2}$$

The case $Re = 0$:. First we consider the case $Re = 0$. In this case, Fourier transformation of the last equation of (B.1) leads to the relation

$$0 = -\xi^2\hat{w}(\xi) + \delta\left(m\delta_\xi - \hat{\rho}(\xi)\right),$$

where δ_ξ is the delta function. Thus we can replace $\hat{w}$ in the last equation of (B.2) by

$$\hat{w}(\xi) = \frac{1}{\xi^2}\delta\left(m\delta_\xi - \hat{\rho}(\xi)\right).$$

We obtain a linear ode system of the form

$$\partial_t\boldsymbol{U}(\xi,t) = A(\xi,\delta,D_r)\boldsymbol{U}(\xi,t) + \delta m\delta_\xi\boldsymbol{e}_5,$$

with $\boldsymbol{U} = (\hat{\rho}, \hat{S}_{11}, \hat{S}_{22}, \hat{S}_{33}, \hat{S}_{13})^T$ and

$$A = \begin{pmatrix}
0 & 0 & 0 & 0 & i\xi\\
0 & -6Dr & 0 & 0 & \frac{2}{21}i\xi\\
0 & 0 & -6D_r & 0 & -\frac{4}{7}i\xi\\
0 & 0 & 0 & -6D_r & \frac{2}{21}i\xi\\
-\frac{1}{5\xi}i\delta + \frac{1}{15}i\xi & 0 & -\frac{1}{7}i\xi & 0 & -6D_r
\end{pmatrix}. \tag{B.3}$$

Let $\alpha(A)$ denote the spectral abscissa of the matrix A, i.e.

$$\alpha(A) := \max_j \mathrm{Re}(\lambda_j),$$

where $\lambda_1, \ldots, \lambda_5$ are the eigenvalues of A. The solution $\boldsymbol{U}(\xi, t)$ of the linear system remains bounded provided $\alpha(A) \leq 0$ and $\boldsymbol{U}(\xi, t) \to 0$ as $t \to \infty$ if $\alpha(A) < 0$.

For $D_r = 0$ the eigenvalues of (B.3) are

$$\lambda_{1,2,3} = 0, \quad \lambda_{4,5} = \pm\sqrt{-1635\xi^2 + 2205\delta}.$$

This predicts the instability of density modulations for horizontal waves with a sufficiently small wavenumber but not a wavelength selection mechanism. This agrees with previous findings of Koch and Shaqfeh [19]. We also see that the problem becomes more unstable if we increase δ.

The introduction of Brownian effects in terms of translational difusion (a case which was excluded here by setting $\gamma = 0$) does also not provide a wavelength selection mechanism at the level of linear stability analysis, see Saintillan [26]. If we include Brownian effects in terms or rotational diffusion, i.e. in the case $D_r > 0$, then we don't have such a simple formula for the eigenvalues. However, we computed the spectral abscissa as a function of ξ. The results of these computations are shown in Figure B.1. In all three plots we set $\delta = 1$ and varied the value of D_r. By increasing the value of D_r

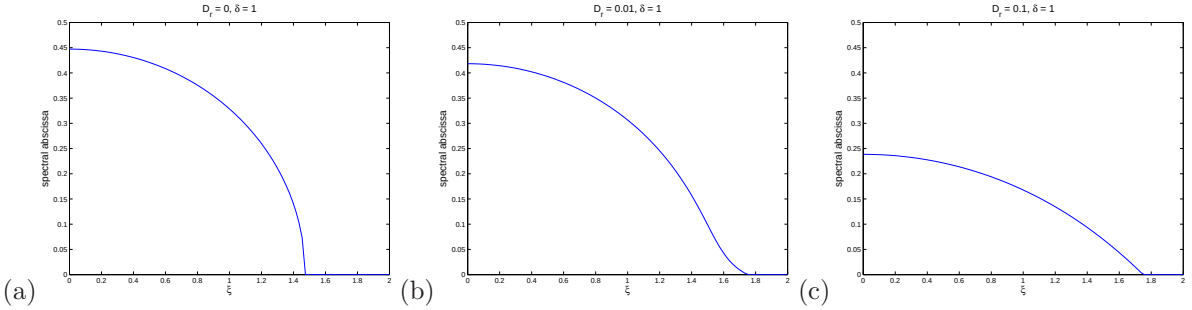

(a) (b) (c)

FIG. B.1. *Spectral abscissa as a function of wavenumber ξ for $\delta = 1$, $Re = 0$ and different values of D_r.*

the problem becomes less unstable. There is no wavelength selection mechanism.

The case $Re > 0$:. Now we consider the case $Re > 0$. Fourier transformation of the linearized equation for w gives

$$Re\partial_t \hat{w}(\xi, t) = -\xi^2 \hat{w}(\xi, t) + \delta(m\delta_\xi - \hat{\rho}(\xi, t)). \tag{B.4}$$

We consider the linear stability of the system (B.2) together with (B.4). This system has the form

$$\partial_t \boldsymbol{U}(\xi, t) = A(\xi, \delta, D_r, Re)\boldsymbol{U}(\xi, t) + \delta m \delta_\xi \boldsymbol{e}_6,$$

with $\boldsymbol{U} = (\hat{\rho}, \hat{S}_{11}, \hat{S}_{22}, \hat{S}_{33}, \hat{S}_{13}, \hat{w})^T$ and

$$A = \begin{pmatrix} 0 & 0 & 0 & 0 & i\xi & 0 \\ 0 & -6Dr & 0 & 0 & \frac{2}{21}i\xi & 0 \\ 0 & 0 & -6D_r & 0 & -\frac{4}{7}i\xi & 0 \\ 0 & 0 & 0 & -6D_r & \frac{2}{21}i\xi & 0 \\ \frac{1}{15}i\xi & 0 & -\frac{1}{7}i\xi & 0 & -6D_r & \frac{1}{5}i\xi \\ -\frac{\delta}{Re} & 0 & 0 & 0 & 0 & -\frac{1}{Re}\xi^2 \end{pmatrix}. \tag{B.5}$$

For $\delta = 0$ and $D_r = 0$, the eigenvalues of A are

$$\lambda_{1,2,3} = 0, \quad \lambda_{4,5} = \pm\frac{1}{105}i\sqrt{1635}\xi, \quad \lambda_6 = -\frac{\xi^2}{Re},$$

and thus the linear system is stable. For $\delta > 0$, we observe instability as well as a wavelength selection. In Figure B.2, we plot the spectral abscissa as a function of ξ for $\delta = 1$, $D_r = 0$ and different values of Re. An increase of Re reduces the spectral abscissa, i.e. it makes the system less unstable. The

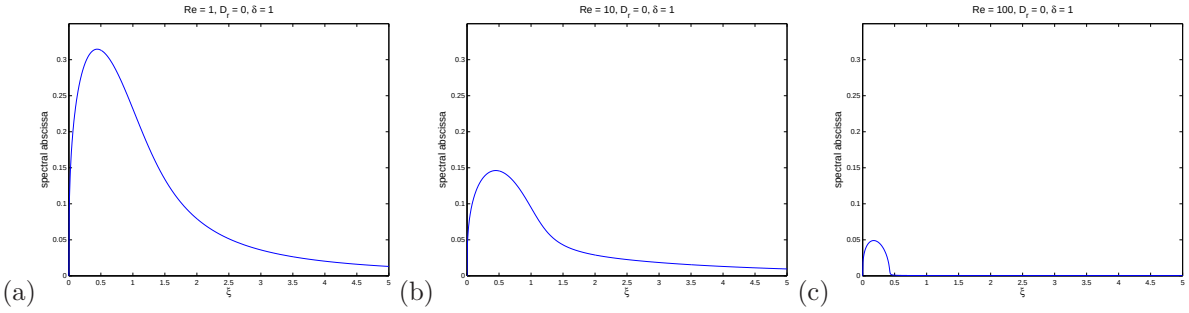

FIG. B.2. *Spectral abscissa as a function of wavenumber ξ for $\delta = 1$, $D_r = 0$ and different values of Re.*

wavelength of the most unstable wave increases (the wavenumber decreases).

As in the case $Re = 0$, an increase of D_r has a stabilising effect, while an increase of δ has a destabilising effect. In addition, an increase of D_r leads to the selection of a longer wavelength, while an increase of δ leads to the selection of a shorter wavelength. In Figure B.3 we show plots of the spectral abscissa vs. the wavenumber for $Re = 1$, $\delta = 1$ and different values of D_r.

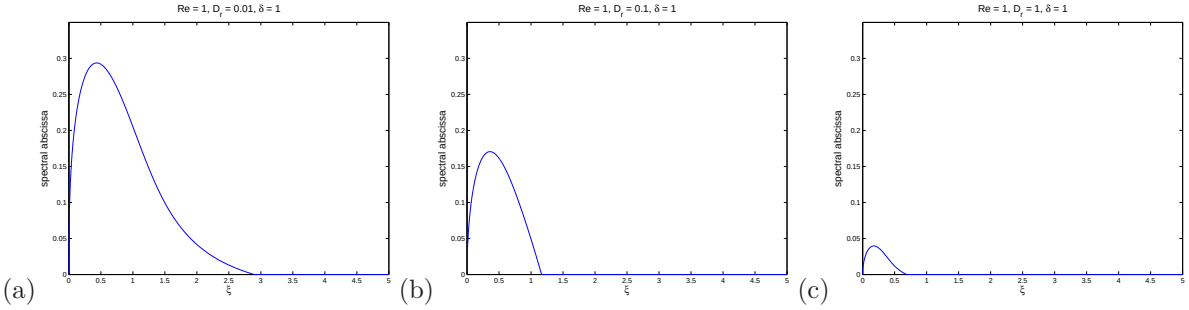

FIG. B.3. *Spectral abscissa as a function of wavenumber ξ for $\delta = 1$, $Re = 1$ and different values of D_r.*

Appendix C. Some remarks about the numerical methods. In this appendix we give some details about the numerical methods, which were used to simulate the three different models for shear flow. For rectilinear flow, the moment closure model and the quasi-dynamic approximation can be discretized using two-dimensional versions of the methods described here.

For each model, the method is based on an operator splitting approach, i.e. during each time step we successively approximate the different components of the coupled system.

We use a staggered grid and discretize the velocity w at the nodes of the grid, i.e. $w^n_{i+\frac{1}{2}} \approx w(x_{i+\frac{1}{2}}, t_n)$ for $i = 0, \dots, m$ and the density ρ at midpoints of a grid cell, i.e.

$$\rho^n_i \approx \frac{1}{\Delta x} \int_{x_{i-\frac{1}{2}}}^{x_{i+\frac{1}{2}}} \rho(x, t_n) dx \approx \rho(x_i, t_n) \quad i = 1, \dots, m.$$

Each subproblem is discretized using either a second order accurate finite volume or a second order accurate finite difference method. The update of w is computed using the Crank-Nicolson method for periodic solutions.

For the full model (4.28), the evolution of f is split into the subproblems

$$\partial_t f + \nabla_{\boldsymbol{n}} \cdot \left(P_{\boldsymbol{n}^\perp}(0, 0, n_1 w_x)^T f \right) = \Delta_{\boldsymbol{n}} f \tag{C.1}$$

and

$$\partial_t f - \partial_x (n_1 n_3 f) = 0. \tag{C.2}$$

Recall that $f = f(x, t, \boldsymbol{n})$. Thus, subproblem (C.1) is a drift diffusion equation on the sphere, which needs to be solved at all the discrete positions $x_1, \ldots, x_m$. In our example, we solve during each time step 400 times this drift diffusion equation on the sphere ($m = 400$). In each case we need to use another value for w_x, i.e.

$$w_x(x_i, t_n) = \frac{w^n_{i+\frac{1}{2}} - w^n_{i-\frac{1}{2}}}{\Delta x}, \quad i = 1, \ldots, m.$$

To discretize (C.1) at a point x_i, we use the sphere grid from [4]. In this approach, a single rectangular computational domain (discretized with an equidistant Cartesian mesh) is mapped to the sphere. In our simulations, the sphere was discretized by mapping a rectangular Cartesian mesh with 60×30 grid cells to the sphere. This means that the position vector $\boldsymbol{n}$ is discretized at 1800 discrete points on the sphere, which are denoted by $\mathbf{n}_{j,k}$, $j = 1, \ldots, 60$, $k = 1, \ldots, 30$.

In [4], it was shown how LeVeque's wave propagation method [20] can be used to discretized hyperbolic pdes on the sphere. A version of the wave propagation algorithm was here used to discretize

$$\partial_t f + \nabla_{\boldsymbol{n}} \cdot \left(P_{\boldsymbol{n}^\perp}(0, 0, n_1 w_x)^T f \right) = 0.$$

Diffusion on the sphere, i.e. the subproblem

$$\partial_t f = \Delta_{\boldsymbol{n}} f,$$

was approximated using a finite volume method for parabolic problems on surfaces, see [3].

Finally, we discretize the transport equation (C.2) for all discrete representations of the position vector $\boldsymbol{n}$ on the sphere. Note that for fixed values of j and k, $n_1 n_2$ in (C.2) is constant. To discretize (C.2), we solve an advection equation for each choice of j and k, i.e. in our test simulations we solved during each time step 1800 advection equations, each with a different advection speed. Each of these advection equations was discretized on a grid with 400 grid cells (the number of grid cells used to discretize the macroscopic space). We used again the high-resolution wave propagation algorithm to approximate these advection problems.

Compared to the full system, the discretization of the effective equation (4.29) as well as the discretization of the linear model (4.30) is simple and computationally much less expensive. The evolution equation for ρ in the effective equation (4.29) is a combination of the wave propagation algorithm for an advection problem with spatially varying advection speed and a finite difference discretization for the nonlinear diffusion term. To discretize the linear moment closure model (4.30), we note that the evolution of $\rho, S_{11}, S_{22}, S_{33}, S_{13}$ can be formulated as a linear hyperbolic system with source term. For its discretization, we use the wave propagation algorithm for linear hyperbolic systems together with an ODE solver for the source term.

In the rectilinear flow case, the evolution of ρ in the quasi-dynamic approximation is approximated by a two-dimensional version of the wave propagation algorithm for scalar transport equations with spatially varying flux function and a finite-difference approach for the diffusion term. The approximation of the nonlinear moment closure system combines the use of the wave propagation algorithm for multidimensional linear hyperbolic systems with an ode solver for the source terms.

Acknowledgements. The authors express their thanks to Professor Felix Otto for his valuable comments and his involvement in several discussions concerning this work, and to Professor Jian-Guo Liu for helpful remarks. Research supported in part by the King Abdullah University of Science and Technology (KAUST), by the project ACMAC of the FP7-REGPOT-2009-1 program of the European Commission, and by the Aristeia program of the Greek Secretariat for Research.

REFERENCES

[1] A.Blanchet, J.Dolbeault, and B.Perthame. Two-dimensional keller-segel model: optimal critical mass and qualitativ properties of the solutions. *Electron. J. Differential Equations*, 44:1–33, 2006.

[2] J.E. Butler and E.S.G. Shaqfeh. Dynamic simulation of the inhomogeneous sedimentation of rigid fibers. *J. Fluid. Mech.*, 468:205–237, 2002.

[3] D.A. Calhoun and C. Helzel. A finite volume method for solving parabolic equations on logically cartesian curved surface meshes. *SIAM J. Sci. Comput.*, 31:4066–4099, 2009.

[4] D.A. Calhoun, C. Helzel, and R.J. LeVeque. Logically rectangular grids and finite volume methods for pdes in circular and spherical domains. *SIAM Review*, 50:723–752, 2008.

[5] M. Doi and S.F. Edwards. *The Theory of Polymer Dynamics*. Oxford University Press, 1986.

[6] Y. Dolak and C. Schmeiser. The Keller-Segel model with logistic sensitivity function and small diffusion. *SIAM J. Appl. Math.*, 66:286–308, 2006.

[7] K.D. Elworthy. *Geometric aspects of diffusions on manifolds*. École d' Été de Probabilités de Saint-Flour XVXVII, 1985-87, 277-425, Lecture Notes in Math., 1362, Springer, Berlin, 1988.

[8] E. Guazzelli and J. Hinch. Fluctuations and instability in sedimentation. *Annu. Rev. Fluid Mech.*, 43:97–116, 2011.

[9] K. Gustavsson and A.K. Tornberg. Gravity induced sedimentation of slender fibers. *Phys. Fluids*, 21:123301, 2009.

[10] S. Helgason. *Groups and Geometric Analysis, Integral Geometry, Invariant Differential Operators and Spherical Functions*. Academic Press, 1984.

[11] C. Helzel and F. Otto. Multiscale simulations for suspensions of rod-like molecules. *J. Comput. Phys.*, 216(1):52–75, 2006.

[12] M.A. Herrero and J.J.L. Velazquez. Singularity patterns in chemotaxis models. *Math. Ann.*, 306:583–623, 1996.

[13] B. Herzhaft and É. Guazzelli. Experimental study of the sedimentation of a dilute fiber suspension. *Physical Review Letters*, 77:290–293, 1996.

[14] B. Herzhaft and É. Guazzelli. Experimental study of the sedimentation of dilute and semi-dilute suspensions of fibers. *J. Fluid Mech.*, 384:133–158, 1999.

[15] E.J. Hinch and L.G. Leal. Constitutive equations in suspension mechanics. Part 1. General formulation. *J. Fluid Mech.*, 71:481-495, 1975.

[16] E.J. Hinch and L.G. Leal. Constitutive equations in suspension mechanics. Part 2. Approximate forms for a suspension of rigid particles affected by Brownian rotations. *J. Fluid Mech.*, 76:187-208, 1976.

[17] E.P. Hsu. *Stochastic Analysis on Manifolds*. Graduate Studies in Mathematics, Vol 38, Amer. Math. Society, Providence, RI, 2002.

[18] W. Jaeger and S. Luckhaus. On explosions of solutions to a system of partial differential equations modeling chemotaxis. *Trans. Amer. Math. Soc.*, 329:819–824, 1992.

[19] D.L. Koch and E.S.G. Shaqfeh. The instability of a dispersion of sedimenting spheroids. *J. Fluid Mech.*, 209:521–542, 1989.

[20] R.J. LeVeque. *Finite Volume Methods for Hyperbolic Problems*. Cambridge University Press, 2002.

[21] B. Metzger, J.E. Butlerz, and E. Guazzelli. Experimental investigation of the instability of a sedimenting suspension of fibers. *J. Fluid Mech.*, 575:307–332, 2007.

[22] M.Renardy. Mathematical analysis of viscoelastic fluids. In *Handbook of differential equations: evolutionary equations*, volume IV, pages 229–265. Elsevier/North-Holland, 2008.

[23] F. Otto and A. Tzavaras. Continuity of velocity gradients in suspensions of rod-like molecules. *Comm. Math. Phys.*, 277(3):729–758, 2008.

[24] B. Perthame. Comment: Flux-limiting equations arising in biology. *Physics of Life Reviews*, 10:476–477, 2013.

[25] D. Saintillan, S. Darve, and S.G. Shaqfeh. A smooth particle-mesh ewald algorithm for stokes suspension simulations: The sedimentation of fibers. *Phys. Fluids*, 17:033301, 2005.

[26] D. Saintillan, S.G. Shaqfeh, and E. Darve. The grows of concentration fluctuations in dilute dispersions of orientable and deformable particles under sedimentation. *J. Fluid Mech.*, 553:347–388, 2006.

[27] Y. Shizuta and S. Kawashima. Systems of equations of hyperbolic-parabolic type with applications to discrete boltzmann equation. Hokkaido Math. J., 14:249–275, 1985.

[28] E.M. Stein and G.L. Weiss. *Introduction to Fourier Analysis on Euclidean Spaces*. Princeton University Press, 1971.

[29] A.K. Tornberg and K. Gustavsson. A numerical method for simulations of rigid fiber suspensions. *J. Comput. Phys.*, 215:172–196, 2006.

[30] M. Verbeni, O. Sánchez, E.Mollica, I. Siegl-Cachedenier an A. Carleton, I. Guerrero, A. Ruiz i Altaba, and J. Soler. Morphogenetic action through flux-limited spreading. *Physics of Life Reviews*, 10:457–475, 2013.

[31] J. Wang and A. Layton. Numerical simulations of fiber sedimentation in Navier-Stokes flows. *J. Comput. Phys.*, 5:61–83, 2009.